Published in final edited form as:
Nat Struct Mol Biol. 2018 November ; 25(11): 1035–1046. doi:10.1038/s41594-018-0143-4.

SAMMSON fosters cancer cell fitness by enhancing concertedly mitochondrial and cytosolic translation

Vendramin Roberto[1,2,3], **Verheyden Yvessa**[1], **Ishikawa Hideaki**[4], **Goedert Lucas**[1], **Nicolas Emilien**[5], **Saraf Kritika**[5], **Armaos Alexandros**[6], **Delli Ponti Riccardo**[6], **Izumikawa Keiichi**[4], **Mestdagh Pieter**[7,8], **Lafontaine L.J. Denis**[5], **Tartaglia Gian Gaetano**[6], **Takahashi Nobuhiro**[4], **Marine Jean-Christophe**[2,3], and **Leucci Eleonora**[1,*]

[1]Laboratory for RNA Cancer Biology, Department of Oncology, KULeuven, Herestraat 49, 3000 Leuven, Belgium

[2]Laboratory For Molecular Cancer Biology, Department of Oncology, KULeuven, Herestraat 49, 3000 Leuven, Belgium

[3]Laboratory For Molecular Cancer Biology, Center for Cancer Biology, VIB, Herestraat 49, 3000 Leuven, Belgium

[4]Department of Applied Biological Science, Global Innovation Research Organizations, Tokyo University of Agriculture and Technology, 3-5-8 Saiwai-cho, Fuchu, Tokyo 183-8509, Japan

[5]RNA Molecular Biology, Center for Microscopy and Molecular Imaging, Université Libre de Bruxelles (ULB), Rue des Professeurs Jeener et Brachet 12, 6041 Charleroi, Belgium

[6]Centre for Genomic Regulation (CRG), University Pompeu Fabra (UPF) and Catalan Institution for Research and Advanced Studies (ICREA), Dr Aiguader 88 08003, Barcelona Spain

[7]Center for Medical Genetics, Gent University, De Pintelaan 185, 9000 Gent, Belgium

[8]Cancer Research Institute Gent, Gent University, De Pintelaan 185, 9000 Gent, Belgium

Abstract

*Corresponding Author.

Data availability statement

The small RNA sequencing data upon SAMMSON KD has been submitted to NCBI Sequence Read Archive (SRA accession: SRP151840) and can be accessed via the following link: https://www.ncbi.nlm.nih.gov/sra/SRP151840. Source data and statistical analysis for figures 1a, 1b, 1d, 1e, 2a, 2c, 2e, 2f, 3a, 3d, 3f, 3h, 4c, 4e, 5c, 6d, 6g, 6h, 7b-g are available in the online version of the paper. All the data that support the findings of this study are available from the corresponding author upon request.

Author Contributions

EL and RV performed most experiments. YV performed experiments described in Figure 2f. EN and SK performed nuclear rRNA northern blot (Fig. 5b and Supplementary Fig. 4a). RDP and AA run RNA secondary structure prediction and *in silico* binding (Fig. 4f). PM performed small RNA-seq (Fig. 5d and Supplementary Fig. 4d). IH and IK performed the experiments in Figure 4g-i and Supplementary Fig. 4c. LG helped for figure 5a and 6a and for additional experiments provided to the reviewers and not included in the final manuscript. DL and GGT and NT helped in the interpretation of the data. EL and RV designed the study. JCM and EL wrote the manuscript with inputs from all the authors.

Competing Interests Statement

The authors declare that they have no conflict of interest.

Europe PMC Funders Author Manuscripts

Synchronisation of translation rates between the mitochondria and their cellular host is critical for the maintenance of cellular fitness, with cancer cells being especially vulnerable to translation uncoupling. Although alterations of cytosolic protein synthesis are common in human cancer, the compensating mechanisms in place in the mitochondria remain elusive. Here we show that the malignant lncRNA *SAMMSON* promotes a balanced increase in rRNA maturation and protein synthesis in the cytosol and mitochondria by modulating the localisation of CARF, an RNA-binding protein sequestering XRN2 in the nucleoplasm and limiting nucleolar rRNA maturation. *SAMMSON* interferes with XRN2 binding to CARF in the nucleus by favouring the formation of an aberrant cytoplasmic RNA-protein complex containing CARF and p32, a mitochondrial protein required for the processing of the mitochondrial rRNAs. This data highlights how a single oncogenic lncRNA can simultaneously modulate RNA-protein complex formation in two distinct cellular compartments to promote cell growth.

Introduction

Highly proliferating cells, such as cancer cells, have an elevated metabolic demand for protein synthesis1. The vast majority of proteins is produced in the cytosol and depends on the correct assembly of ribosomes. Ribosome biogenesis requires the activity of all 3 nuclear RNA polymerases 2. Whereas the biogenesis of ribosomal proteins is initiated in the nucleus by the RNA polymerase II, maturation of a polycistronic precursor generated by RNA pol I in the nucleolus, gives rise to 18S, 28S and 5.8S rRNAs that are subsequently modified and processed by hundreds of small nucleolar RNAs (snoRNAs) and protein cofactors into their mature forms. The *5S* rRNA instead, is transcribed independently in the nucleoplasm by the RNA pol III3.

The synthesis of 13 of the mitochondrial membrane proteins engages a dedicated set of ribosomes, or mitoribosomes, whose biogenesis requires active transcription by the mitochondrial polymerase (mtRNAP) to produce the mitochondrial rRNAs precursor that is then cleaved by RNase H and p32 to produce the mature 12S and 16S4. (Mito)ribosome biogenesis is the most energy-consuming cellular process3 and it is therefore tightly regulated by growth and stress signalling pathways5–8.

Apart from the aforementioned 13 membrane peptides, the majority of the mitochondrial proteome is encoded by the nuclear genome and synthesized in the cytosol as precursor proteins that are ultimately imported into mitochondria9. Thus, a fully functional Oxidative Phosphorylation chain requires proteins translated by both mitochondrial and cellular machineries. The two translation apparatuses therefore need to be synchronized and tightly regulated to respond to environmental cues in a coordinated fashion. Accordingly, desynchronization through disruptions of mitochondrial protein synthesis impacts cell proliferation and fitness10–12 thus highlighting the existence of intracellular circuit(s) that couple mitochondrial translation to cell proliferation13. In yeast, mitochondrial protein synthesis defects cause mitochondrial membrane depolarization thus impairing the import of nuclear-encoded mitochondrial precursors. These accumulate in the cytosol to induce a proteotoxic stress response, known as mPOS14,15. Similarly to mitochondrial translation, cytosolic protein synthesis is tightly linked to cell proliferation and under direct control of

oncogenes and tumour suppressors16. Increasing evidence indicates that oncogenes can stimulate the translation rates in the cytosol and mitochondria. However, how cancer cells ensure that the proper balance between the output of the two protein synthesis machineries is maintained remains unclear.

One example of an oncogene with a direct role in control of translation is the transcription factor Myc, that directly increases protein synthesis rates in the cytosol by controlling the expression of multiple components of the protein synthetic machinery17. Myc is also capable of enhancing the activity of the mitochondrial protein synthesis machinery. p32, a mitochondrial protein required for the maturation of mitochondrial rRNAs, is a direct transcriptional target of Myc 18. Attenuation of p32 expression reduces growth rate of glioma cells expressing Myc and impairs tumour formation *in vivo*18. Several mitochondrial ribosomal proteins were also identified as Myc targets and, among them, Ptcd3 (Pentatricopeptide Repeat Domain 3) was shown to have a critical role in the maintenance of B-cell lymphomas12. This data raises the possibility that key oncogenes can directly contribute to the maintenance of the necessary synchronisation of the two protein synthesis machineries.

We recently described *SAMMSON*, a lineage-specific lncRNA aberrantly expressed in a large fraction (>90%) of cutaneous melanoma. Strikingly, melanoma cells are addicted to *SAMMSON*, irrespective of their genetic make-up or transcriptional state and they quickly undergo apoptosis upon its inhibition19. We showed that *SAMMSON* interacts with p32 and promotes its efficient targeting to mitochondria19. Accordingly, *SAMMSON* depletion caused mitochondrial protein synthesis defects resulting in membrane depolarization and activation of a mPOS-like response19. It therefore remains unclear whether *SAMMSON* itself is capable of -concomitantly- provoking an adaptive cytosolic response to ensure a coordinated increase of the cytosolic and mitochondrial translation rates or whether this is driven by *SAMMSON*-independent mechanisms.

To address this we searched for new *SAMMSON*-interacting proteins and identified XRN2 (5’-3’Exoribonuclease 2) and CARF (Collaborator of ARF, the product of the *CDKN2AIP* gene), two proteins known to play key roles in the biogenesis of cellular ribosomes. XRN2 is a 5’-3’ exoribonuclease with a crucial role in the maturation of virtually all RNA species and in nuclear RNA turnover. In the nucleoplasm, XRN2 participates in 3’-end processing of mRNA20 and in the degradation of several tRNAs including the initiator tRNA(Met) in stress conditions21,22. In the nucleoli, XRN2 is essential for the processing of snoRNA ends2,23,24 and for the degradation of spacer fragments that are excised during rRNA maturation, thus ensuring proper maturation of the 5.8S and 28S rRNAs2,25.

XRN2 access to the nucleoli is dynamically regulated by CARF, which titrates XRN2 excess by retaining it in the nucleoplasm to fine-tune pre-rRNA maturation26. Accordingly, CARF overexpression impairs rRNA processing26.

Here we show that *SAMMSON* promotes CARF binding to p32 thus interfering with its binding to XRN2. This favours XRN2 localization to the nucleoli and p32 targeting to mitochondria and thereby the stimulation of rRNA biogenesis and protein synthesis in both

compartments. By boosting translation, *SAMMSON* confers a growth advantage to immortalised cells irrespective of their tissue of origin.

Results

SAMMSON increases the tumorigenic potential in a lineage-independent fashion

We established that melanoma cells are addicted to *SAMMSON* independently of their genetic make-up19. As *SAMMSON*'s expression becomes readily detectable at the early stages of melanomagenesis19, we asked whether a causative link exists between its expression and malignant transformation. We tested the effects of ectopic *SAMMSON* expression on immortalized Mel-ST cells belonging to the melanocytic lineage27 (Supplementary Fig. 1). Ectopic expression of *SAMMSON* under the control of a PGK promoter using a lentiviral-based approach, conferred growth advantage *in vitro* (Supplementary Fig. 1a-d) and allowed tumour growth in nude mice, indicating that its presence is sufficient to transform immortalized cells of melanocytic origin (Supplementary Fig. 1e-g).

SAMMSON also conferred a growth advantage to cells that do not belong to the melanocytic lineage, namely the immortalized Lymphoblastoid Cell Line (LCL; *SAMMSON*-negative) (Fig.1a and b). Ectopic *SAMMSON* expression in these cells cooperated with the Large T Antigen (LTA) in promoting transformation (Fig. 1c-e). The combined expression of *SAMMSON* and LTA led to an increase in growth which significantly exceeded that of the LTA alone (Fig. 1b). Moreover, while control LCLs were unable to grow in soft agar, LCLs expressing both *SAMMSON* and LTA were capable of forming more and larger colonies than LCL cells expressing LTA alone (Fig. 1c-e). These findings demonstrated the ability of *SAMMSON* to enhance malignant transformation within and outside the melanocytic lineage.

Desynchronization of cytosolic and mitochondrial translation machinery is detrimental and can be exploited therapeutically

We established that Knock Down (KD) of *SAMMSON* decreases melanoma viability by impairing mitochondrial translation and inducing an mPOS-like response19. This finding suggested that disruption of the equilibrium between cytosolic and mitochondrial protein synthesis impairs melanoma cell fitness13. Accordingly, acute depletion of *SAMMSON* using AntiSense Oligonucleotides (ASOs)19 in the established melanoma line SK-MEL-28 (Fig. 2a) caused severe defects in mitochondrial protein synthesis (Fig. 2b and c) and apoptotic responses19 before any impact on cytosolic protein synthesis could be observed (Fig. 2b and c). Both ASOs (Gapmer3 and 11) have previously been selected for their ability to efficiently decrease *SAMMSON* expression without causing any off-target effects19.

Loss of cell viability induced by *SAMMSON* KD was phenocopied by specific inhibition of mitochondria protein synthesis using chloramphenicol (Fig. 2d and e). Designed to target bacterial ribosomes, chloramphenicol and antibiotics of the tetracyclines family are also effective in inhibiting the structurally-related mitoribosomes11,12. Consequently, survival of SK-MEL-28 melanoma cells exposed to chloramphenicol was compromised in a dose-

dependent manner (Fig. 2d and e). This data identified the balance between cytosolic and mitochondrial protein synthesis rates as an exploitable therapeutic vulnerability in melanoma. Accordingly, an antibiotic in clinical use such as Tigecycline sensitized "invasive" (therapy resistant)28 melanoma cells (MM099) to the combination of Dabrafenib and Trametinib (Fig. 2f).

This data demonstrated the importance of a coordinated translation in both compartments and indicated that disruption of mitochondrial translation is a valuable antimelanoma strategy.

SAMMSON interacts with CARF and XRN2, two proteins involved in ribosome biogenesis

Given that expression of *SAMMSON* is sufficient to promote malignant transformation and that cancer cell fitness depends on a synchronized increase in protein translation in the mitochondria and cytosol we hypothesized that *SAMMSON* may also control cytosolic translation. A search in our list of putative *SAMMSON's* interacting partners19 identified XRN2 and CARF, two proteins implicated in ribosome biogenesis in the nucleus. Both proteins showed elevated expression in melanoma compared to normal human epidermal melanocytes (NHEM; Supplementary Fig. 2a). We confirmed the ability of *SAMMSON* to interact with these proteins using RNA pull-downs (PD) and RNA ImmunoPrecipitations (RIP). By specifically pulling-down *SAMMSON* using a pool of antisense oligonucleotides in native (Fig. 3a and b) and crosslinking conditions (Supplementary Fig. 2b), we observed a robust enrichment for CARF and XRN2 (Fig. 3b and Supplementary Fig. 2b). In contrast other abundant proteins such as vinculin or the RNA-binding protein SFRS1 could not be detected (Fig. 3b and Supplementary Fig. 2b). Additionally, no enrichment for these proteins was observed when performing the assay in the *SAMMSON*-negative mouse cell line p38 (Fig. 3c). Conversely, the lncRNA *MALAT1* an established SFRS1-partner29, but not *SAMMSON*, was identified in SFRS1-immunoprecipitates (Fig. 3d and e). Likewise, RNA fractions obtained from XRN2 and CARF immunoprecipitates (Fig. 3g and i) were enriched in *SAMMSON,* but not in the cytosolic RNAs *TBP* and *HPRT* (Fig. 3f-h). Further confirming the interaction, *TERRA,* a known XRN2 substrate30, was retrieved in XRN2, but not in CARF immunoprecipitates. In contrast, CARF, but not XRN2, associated specifically with another melanoma-specific lincRNA (*LINC00698*). This data validated CARF and XRN2 as *bona fide SAMMSON*-interactors.

Consistent with previous findings, CARF and XRN2 co-immunoprecipitated (Fig. 3g and i) confirming their physical interaction21. This observation raised the possibility that *SAMMSON* may be engaged into a ribonucleoproteic complex containing both XRN2 and CARF. Alternatively, *SAMMSON* may interact with both proteins independently, and even possibly modulate the XRN2-CARF association. To address this, we mapped the XRN2-*SAMMSON*'s interaction interface using three different HA-tagged XRN2-deletion constructs26 (Fig. 4a). An interaction between *SAMMSON* and wild-type XRN2 was readily detected by RIP assays (Fig. 4b and c). Although *SAMMSON* did interact with the N1 form of XRN2, which lacks the last 270 amino acids, further deletion of another 171 amino acids containing an evolutionarily conserved region (mutant N2), abrogated the

binding. Interestingly, this conserved domain was also required for the interaction between XRN2 and CARF (Fig. 4b and c)28.

Similarly to CARF, *SAMMSON* was also incapable of binding a XRN2 mutant lacking the first 152 amino acids (mutant C), which constitutes a large part of the catalytic domain. In contrast another ncRNAs such as the 18S, known to be an XRN2 substrate25, required an intact carboxy-terminal half of the protein for binding, and did not occupy the catalytic substrate (Fig. 4c). These observations indicated that *SAMMSON* may modulate XRN2 functions rather than being a direct XRN2 substrate. In keeping with this, silencing XRN2 stabilised *TERRA*, a known XRN2 substrate but did not affect *SAMMSON* levels (Fig. 4d and e).

In order to identify which portion of *SAMMSON* is responsible for binding to XRN2, CARF and p32, we predicted their interactions *ab initio* using *cat*RAPID31. *cat*RAPID predicted an interaction interface with all three proteins located in a region comprising the last 400-300 nucleotides of *SAMMSON* (Fig. 4f). Based on these findings, we designed two *SAMMSON* deletion mutants in which we inserted a RAT (RNA Affinity in Tandem)-tag (Fig. 4g). The aptamer recognising the RAT-tag was FLAG-conjugated thus allowing us to purify *SAMMSON*-containing complexes with an anti-FLAG antibody. The experiment (Fig. 4h) confirmed the *in silico* predictions, since deletion of the last 500 nucleotides in *SAMMSON* sequence impaired its ability to interact with all the proteins (Fig. 4i). This data indicated that the 3'-end of *SAMMSON* is engaged in multiple protein interactions.

SAMMSON modulates XRN2 localization and nucleolar functions

CARF regulates XRN2 access to the nucleoli (and related functions) by tethering it into the nucleoplasm26. To further investigate the relationship between XRN2, CARF and *SAMMSON,* we determined the localization of CARF and XRN2 upon *SAMMSON* KD. Immunofluorescent staining revealed that *SAMMSON* silencing led to the complete exclusion of XRN2 from the nucleoli (Fig. 5a) and re-location of the cytoplasmic fraction of CARF to the nucleoplasm (Supplementary Fig. 3a).

To rule out the possibility that the nucleoplasmic relocation of XRN2 was an indirect consequence of the mitochondrial stress triggered by *SAMMSON* KD19, we interfered with mitochondrial translation via a distinct mechanism32 by treating the cells with chloramphenicol and determined XRN2 localization (Supplementary Fig. 3b and c). This confirmed that XRN2 localization was not affected by this treatment (Supplementary Fig. 3b and c). Moreover, XRN2 localization was also unaffected by the silencing of *NEAT1*, another lncRNA reported to interact with XRN233 and implicated in stress responses34 (Supplementary Fig. 3d and e). Hence, the displacement of XRN2 from the nucleoli is a direct consequence of *SAMMSON*'s silencing.

XRN2 modulates the biogenesis of the cytosolic ribosome by processing the rRNA and snoRNA in the nucleolus. Displacement of XRN2 away from the nucleoli in *SAMMSON*-depleted cells indicated that *SAMMSON* is likely to modulate XRN2 nucleolar functions. Similar to XRN2 KD, *SAMMSON* KD caused the accumulation of an aberrant precursor, the 34S pre-rRNA, which arises from the inhibition in the cleavage of the 5'-ETS (External

Transcribed Spacer; Fig. 5b and Supplementary Fig. 4a). Processing in the 5'-ETS and turnover of the cleaved fragments are intimately connected35. Accordingly, inhibition of the cleavage increased the amount of the fragment +1-01 (Fig. 5b and Supplementary Fig. 4a). As a consequence, we observed an imbalanced production of 18S (Fig. 5c and Supplementary Fig. 4b). Moreover, consistent with previous data showing impaired mitochondrial targeting of p32 and defective mitochondrial rRNA processing19, levels of mitochondrial rRNAs (12S and 16S) were also decreased (Fig. 5c and Supplementary Fig. 4b) while the expression of mitochondrial rRNA precursors slightly increased as a result of the defective processing (Supplementary Fig. 4c). Conversely, other mitochondrial transcripts remained unaffected (Fig. 5c and Supplementary Fig. 4b).

Nucleolar XRN2 is also implicated in the maturation of the 5'-ends of snoRNAs2,23,24. SnoRNAs are largely encoded in host gene introns and produced by endo- and exoribonucleolytic digestion of spliced-lariats36,37. Consistently, we detected aberrant 5' extended forms of snoRNA precursors upon *SAMMSON* silencing (Fig. 5d). Note that the processing of the 3'-end of snoRNA precursors was also affected. This may indicate that XRN2-mediated 5'-end processing is required for subsequent trimming of the 3'-end.

In addition to its nucleolar functions XRN2 also exhibits a nucleoplasmic function linked to translation, such as the processing and degradation of initiator tRNAMet21. Consistent with the complete re-localization of XRN2 into the nucleoplasm, a decreased expression of the initiator tRNA for methionine (tRNA61-MetCAT) was observed upon *SAMMSON* depletion (Supplementary Fig. 4d). This data indicated that *SAMMSON* favours XRN2 localization to nucleoli and promotes its ability to support ribosome biogenesis.

SAMMSON rewires the melanoma RNA-binding protein network involved in ribosome biogenesis

XRN2 exclusion from the nucleoli and its increased co-localisation with CARF in the nucleoplasm upon *SAMMSON* KD indicated that *SAMMSON* may interfere with CARF binding to XRN2. However, while *SAMMSON* is predominantly cytoplasmic19, XRN2 is exclusively nuclear. CARF instead, has been detected in both the nucleoplasm, where the interaction with XRN2 takes place26, and the cytoplasm, where its function remains unclear (Fig. 6a). Consistently, a pool of CARF was detected in the cytoplasm of melanoma cells (Fig. 6a). Immunostaining for CARF and p32, another validated *SAMMSON*'s interacting partner19, indicated that the two proteins co-localised in the cytoplasm of melanoma cells and their co-localization was lost upon silencing of *SAMMSON*, when CARF relocated to the nucleus (Fig. 6a). Consistent with our findings showing that *SAMMSON* promotes mitochondrial targeting of p3219, *SAMMSON*'s depletion also affected the localization of p32 that diffusely localized to the cytoplasm and partly to the nucleus in *SAMMSON* KD cells (Supplementary Fig. 5a).

We then investigated the possibility that *SAMMSON*, CARF and p32 are engaged into a ribonucleoprotein complex. We performed RIP using melanoma cell extracts supplemented with RNase A (Fig. 6b). While p32 was readily detectable in CARF immunoprecipitates in absence of RNase A treatment, this interaction was abrogated in the presence of RNase A (Fig. 6b). Similar results were obtained with Proximity Ligation Assay (PLA) for CARF and

p32 (Supplementary Fig. 5b). Conversely, similar RIP experiments in LCLs, which do not express *SAMMSON,* failed to detect an association between CARF and p32 (Fig. 6c and Supplementary Fig. 5c). This data indicated that p32 and CARF interact specifically in melanoma cells and in an RNA-dependent manner. To test whether this interaction is mediated by *SAMMSON* itself, we used LCLs and assessed binding between CARF and p32 using RIP assays (Fig. 6c and Supplementary Fig. 5c respectively). Ectopic expression of *SAMMSON* alone was sufficient to trigger the binding between CARF and p32 and promoted export of a fraction of CARF to the cytoplasm (Supplementary Fig. 5d). Accordingly, KD of CARF affected the mitochondrial network architecture (Supplementary Fig. 6a).

Moreover, PLA in Mel-ST expressing *SAMMSON* ectopically further confirmed that the interaction is *SAMMSON*-dependent (Supplementary Fig. 6b).

Conversely, RIP for CARF showed increased binding of XRN2 to CARF in *SAMMSON* KD cells and this occurred at the expense of CARF-p32 interaction (Fig. 6d and e and Supplementary Fig 6c and d). PLA further confirmed that *SAMMSON* silencing decreases the number of interactions between CARF and p32 (Fig. 6f-h).

These findings established that *SAMMSON's* expression is sufficient to trigger an "aberrant" interaction between CARF and p32 to promote CARF re-localization to the cytoplasm. Remarkably, ectopic expression of *SAMMSON* was sufficient to drive this interaction even in cells that are not derived from the melanocytic lineage.

SAMMSON promotes translation in both the cytosol and mitochondria

This data indicated that *SAMMSON* may stimulate ribosome biogenesis to concertedly increase mitochondrial and cytosolic translation. Consistently, ectopic expression of *SAMMSON* in the immortalized human Mel-ST cells resulted in an increased amount of nuclear rRNA (Fig. 7a and Supplementary Fig. 7a). *SAMMSON* expression also resulted in global increase in *de novo* translation rates in both cytosolic and mitochondrial compartments, as illustrated by puromycin incorporation assay (SUnSET38) (Fig. 7b and Supplementary Fig. 7b). Importantly, the increase in translation was detectable 30h after transfection, before any significant impact on cell proliferation could be measured (48h time point; Fig. 1b and Supplementary Fig. 1b). This observation rules out the possibility that the increase in translation rate is a consequence of increased cell proliferation. Increased translation was also detected in Mel-ST xenografts (Fig. 7g and Supplementary Fig. 7f and g). Similar results were obtained in the LCLs transduced with *SAMMSON* and the LTA (Fig. 1). Overexpression of *SAMMSON,* but not LTA alone, induced a robust increase in translation in both compartments (Fig. 7c and Supplementary Fig. 7c). This result was further confirmed by metabolic labelling with AHA followed by extraction of mitochondria in proteinase K upon *SAMMSON* overexpression, thus indicating that the increased signal was unlikely to derive from cytosolic ribosomes attached to the mitochondrial membrane (Supplementary Fig. 7e). Consistent with previous results19, we could not detect any change in *p32* mRNA expression (Fig. 7d), however its protein levels in the mitochondria were significantly increased (Fig. 7e and f and Supplementary Fig. 7c and d). We concluded that *SAMMSON* is capable of stimulating ribosome biogenesis, and thereby protein synthesis,

by rewiring complex formation and cellular localization of proteins involved in the maturation of nuclear and mitochondrial rRNA.

Discussion

Nucleolar hypertrophy has long-been recognized as an hallmark of cancer39 and changes in nucleolar functions contributes to malignant transformation. Accordingly, several RNA polymerase I inhibitors have been introduced in the clinic and/or enrolled into clinical trials40,41. A growing body of evidence indicates that quantitative and qualitative reprogramming of cytosolic and mitochondrial translation are required to sustain tumour development and progression42. Moreover, cytosolic and mitochondrial protein synthesis machineries need to be balanced to avoid proteotoxic stress14,43,44. While mitochondria are relatively efficient at adjusting their protein synthesis rate to the income in cytosolic proteins44, deregulation of mitochondrial translation invariably induces detrimental responses19,45, due to the higher stability of cytosolic ribosomes and to the multiple regulatory steps downstream of ribosome biogenesis. Our data suggests that disruption of this equilibrium by blocking mitochondrial translation, either by knocking-down lineage-specific lncRNAs such as *SAMMSON* or antibiotics, can be exploited therapeutically to kill cancer cells.

We previously showed that melanoma cells are addicted to *SAMMSON*, a lncRNA interacting with p32 to regulate mitochondrial protein synthesis19. Here we establish *SAMMSON* as a key player in nuclear-mitochondrial communication and a guardian of proteostasis in melanoma, by means of its ability to stimulate rRNA maturation in the nucleoli and increase the rate of cytosolic protein synthesis (Fig. 8).

SAMMSON participates in the reprogramming of the nucleolar activities in melanoma by modulating the subcellular localization of XRN2 (Fig. 8). Through this process, *SAMMSON* stimulates rRNA and snoRNA processing in the nucleoli, stabilizes $tRNA^{Met}$ in the nucleoplasm and ultimately, increases translation in the cytosol, thus increasing cancer cell fitness.

The ability of *SAMMSON* to perturb the formation of a complex between CARF and XRN2 was unexpected considering that the CARF-XRN2 interaction was reported to be RNA-independent26.

Our data indicates that *SAMMSON* may interfere with the formation of the CARF-XRN2 complex via distinct mechanisms. However, the relative contribution of these mechanisms remains to be established.

Since both *SAMMSON* and CARF bind to overlapping domains of XRN2, *SAMMSON* may either mask the CARF binding site or promote (or impair) the deposition of post-translational modifications that affects XRN2 localization and (or) function. In addition, in presence of *SAMMSON*, CARF switches from a nuclear complex with XRN2 to an aberrant complex with p32 into the cytoplasm. CARF cytoplasmic re-localization physically limits its ability to interact with XRN2, which is exclusively nuclear. Compartmentalization, a feature that underlies the difference between eukaryotic and prokaryotic cells, plays a key role in

Europe PMC Funders Author Manuscripts

many biological processes. Accordingly, XRN2 localizes exclusively to the nuclei and exerts specific functions in different sub-nuclear compartments. XRN2 biological activities are therefore strongly dependent upon its compartmentalization rather than specificity in the selection of its substrates.

Overall the rewiring of the RNA-binding protein network increases concomitantly cytosolic and mitochondrial protein synthesis rates (Fig. 8). This rather sophisticated, yet relatively simple, switching mechanism is likely to provide cancer cells with a growth advantage and may therefore be exploited by other oncogenic noncoding RNAs and/or proteins. It will therefore be interesting to assess whether similar mechanisms are at play in other types of cancer.

Although it remains to be formally established that its expression is cancer-specific, it is tempting to speculate that *SAMMSON* is expressed exclusively in melanoma cells as a by-product of aberrant RNA biology. A similar example is provided by a protein-coding gene ΔN-Netrin-1, a variant of Netrin-1 produced by transcription from an internal promoter and detectable only in cancer cells46. In contrast with the Netrin-1 protein, which is secreted, the cancer variant localizes aberrantly to the nucleoli where it affects rRNA processing and nucleolar structure46. Here we show that *SAMMSON* aberrant expression is sufficient to impose CARF binding to p32, stimulate cytosolic and mitochondrial translation and enhance malignancy in a lineage-independent manner. *SAMMSON* could therefore be viewed as a selfish gene, which tries to perpetuate its expression by increasing proliferation of malignant cells through increased translation. All together we showed that the oncogenic lncRNA *SAMMSON* hijacks key RNA-binding proteins to concertedly enhance translation in the cytosol and in the mitochondria. This ensures the maintenance of the equilibrium between the two translation rates, which is so essential for cancer cell survival. Targeting this equilibrium through inhibition of mitochondrial protein synthesis machinery is emerging as a promising antimelanoma strategy.

Methods

Cell culture and transfection

All lines were grown in 5% CO_2 at 37 °C. SK-MEL-28 (a gift from Lionel Larue), SK-MEL-28 BRAFi resistant (a gift from Daniel Peeper), and LCLs (a gift of Lorenzo Leoncini) were grown in RPMI 1640-glutamax (Gibco, Invitrogen) supplemented with 10% FBS (Gibco, Invitrogen). Mel-ST (a gift of Corine Bertolotto) were grown in DMEM-glutamax (Gibco, Invitrogen) supplemented with 7% FBS (Gibco, Invitrogen). HEK293T (from ATCC) were grown in DMEM-glutamax (Gibco, Invitrogen) supplemented with 10% FBS (Gibco, Invitrogen). The patient-derived passages MM cell line (a gift from Ghanem-Elias Ghanem) were grown in F-10 (Gibco, Invitrogen), supplemented with 10% FBS (Gibco, Invitrogen) and 12 mM Glutamax (Gibco, Invitrogen). NHEM (a gift from Hilde Brems) were grown in MGM-4 melanocyte growth medium (Lonza). p38 cells were grown in F-12 media (Gibco, Invitrogen) supplemented with 10% FBS (Gibco, Invitrogen), 2mM Glutamine (Gibco, Invitrogen) and 25 μg mL^{-1} of Hygromycin B (Thermo Fisher Scientific). All cell lines used in this study were mycoplasma negative.

Cells were transfected with Lipofectamine 2000 (Thermo Fisher Scientific) according to manufacturer instructions with 25 nM of non-targeting GapmeR or *SAMMSON*-targeting GapmeR3 or 11 (Exiqon) and collected 30 h after transfection, with 25 nM siCARF (SMART-pool, Dharmacom) or with 50 nM of siXRN2 (Sigma-Aldrich) and collected 72 h after transfection. Cells were transfected with Lipofectamine RNAiMax (Thermo Fisher Scientific) according to the manufacturer instructions with 25 nM of siNEAT1 siPOOLs (siTOOLS Biotech) and fixed 72 h after transfection. Sequences of the GapmeRs and siRNAs are indicated in Supplementary Table 1. For HA-XRN2 constructs transfection, 4 15 cm ∅ plates per construct were transfected with 25 μg plasmid per plate and 70 μL Lipofectamine 2000 per plate and samples were collected 72 h after transfection. HEK293T cells were transfected with standard calcium phosphate method.

Cloning and lentiviral transduction

SAMMSON was described elsewhere19. *SAMMSON* deletion constructs ± RAT-tag were generated as following. *SAMMSON* cDNA fragment was amplified by PCR using primers set HIW885 and HIW886 with the pLenti_PGK_*SAMMSON* plasmid as template. The PCR product was ligated into BamH I-Xho I sites of pcDNA5-FRT-TO vector and resulted product was used for transformation of DH5α competent cells to obtain single clones. Sub-cloned product pcDNA5-FRT-TO-*SAMMSON* was verified by DNA sequencing. For construction of RNA aptamer fused with *SAMMSON*, RAT-tag was amplified by PCR using primer set HIW897 and HIW898 using previously described49 RAT-U1 snRNA expression vector as template. Amplified RAT tag coding fragment was ligated into Xho I-Apa I sites of pcDNA5-FRT-TO-SAMMSON. The resulting product (pcDNA5-FRT-TO-*SAMMSON*_RAT-tag) was verified by DNA sequencing. Using pcDNA5-FRT-TO-*SAMMSON*_RAT-tag as template, *SAMMSON* deletion mutant coding fragments were amplified by PCR with following primers sets: HIW885 and HIW899 for *SAMMSON*-5' half, HIW900 and HIW886 for *SAMMSON*-3' half and HIW901 and HIW886 for *SAMMSON*-3' 500 base, respectively. After removing full-length *SAMMSON* sequence from pcDNA5-FRT-TO-*SAMMSON*_RAT-tag using BamH I-Xho I restriction enzymes, the PCR products were ligated into the same sites. Resultant deletion constructs were verified by DNA sequencing. All primer sequences are indicated in Supplementary Table 1.

HA-XRN2 constructs (WT, C, N1 and N2) were previously described in 26. For *SAMMSON* infection, lentivirus produced in HEK293T cells was used to infect the Mel-ST and LCLs cells. Successfully infected cells were selected in puromycin (InvivoGen, 0.5 μg mL^{-1})-containing medium for 1 week. For SV40 LTA (a gift of Prof. Anna Sablina) infection, lentivirus produced in HEK293T cells was used to infect LCLs cells. Successfully infected cells were selected in hygromycin B (Invitrogen, 100 μg mL^{-1})-containing medium for 1 week to 2 weeks.

Cell growth and cell death assays

Cell growth was measured with CellTiter-Glo luminescent cell viability assay (Promega), Caspase activity was measured using Caspase-Glo 3/7 assay (Promega) with a VIKTOR X4 Reader (PerkinElmer). Tigecycline (Sellekem) was used at a 5, 25 or 50 μM concentration. BRAFi (Dabrafenib-TAFINLAR®, Novartis) and MEKi (Trametinib-MEKINIST®,

Novartis) were used at 10 nM and 2.5 nM concentration respectively. Chloramphenicol (Sigma-Aldrich) was used at a 100, 200 or 400 μg mL^{-1} concentration.

Cell count, colony assays and soft agar assays

For vital counts, cells were stained with Trypan Blue (Sigma-Aldrich) and counted with TC20 automated cell counter (Biorad).

For colony assays, 1×10^3 Mel-ST or SK-MEL-28 cells were plated in six-well plates and cultured for 1 week. The cells were then fixed and stained for 15 min with a 1% crystal violet in 35% methanol solution. Chloramphenicol (Sigma-Aldrich) was used at a 100-200-400 μg mL^{-1} concentration.

For soft agar assay, 1×10^4 cells were embedded in 1 mL of RPMI 1640 containing 10% FBS and 0.35% noble agar (Sigma-Aldrich) on a base layer made of RPMI 1640 containing 10% FBS and 2% noble agar in a well of a 6-well plate. After 2 to 3 weeks of incubation, cells were fixed and stained with a crystal violet solution (0.05% crystal violet, 0.05% methanol and 0.37% PFA) for 2 h.

RAP-WB

For the validation of protein targets, two sets of 48 tiling probes were used to affinity purify mature *SAMMSON* and *HPRT* transcripts (Biosearch Technologies). Briefly, 100 μL of Streptavidin Sepharose High Performance beads (GE Healthcare) were coupled to 400 pmol of biotinylated probes against *SAMMSON* overnight at 4 °C. Cells (6×10^7 cells per sample) were lysed in 2 mL of pull-out buffer (20 mM Tris-HCl pH 7.5, 200 mM NaCl, 2.5 mM $MgCl_2$, 0.05% Igepal, 60 U mL^{-1} Superase-In (Ambion), 1 mM dithiothreitol (DTT) and 1× Halt Protease and Phosphatase Inhibitor Single-Use Cocktail (Life Technologies)) and incubated for 3 h with the beads at 4 °C on a rotating wheel. As a negative control, an additional sample was digested with 10 μg mL^{-1} RNase A for 10 min at room temperature before incubation with *SAMMSON* probes.

For the crosslinking experiments, cells were washed once in PBS, crosslinked dry at 400 mJ cm^{-1} and lysed. Washes were performed in RNase free water.

RIP

RIP was performed as previously described50. p32, XRN2 and CARF were immuno-precipitated using 4 μg of specific antibody (p32, A302-862A, Bethyl Laboratories; XRN2, A301-103A, Bethyl Laboratories; CARF, A303-862A, Bethyl Laboratories) coupled to 35 μL of protein G Dynabeads (Invitrogen) overnight at 4 °C on a rotating wheel.

RNA Aptamer-based Affinity Purification

To identify p32-CARF-XRN2 binding sites on *SAMMSON*, the RAT-tag based method was used49 with slight modifications. Briefly, a mixture of three plasmids was co-transfected into HEK293T cells; one plasmid expressed RAT-tagged *SAMMSON* derivatives, one plasmid y18Sn tagged U2 (pcDdCMV-y18Sn-U251) for transfection control and one plasmid expressed HA-FLAG (HF)-tagged PP7CP (pcDNA3.1-PP7CP-HF) in a 7:2:1 ratio.

24 h post-transfection medium was changed and after 4 hours of incubation cells were collected. The cells were then lysed in lysis buffer (50 mM Tris-HCl pH 8.0, 150 mM NaCl, 2.5 mM $MgCl_2$, 0.5% IGEPAL-CA630, 1 mM PMSF) and incubated on ice for 15 min. The soluble fraction, obtained after centrifugation at 20,000 *x*g for 15 min at 4 °C, was mixed with anti-FLAG-M2-conjugated agarose beads and rotated for 4 h at 4 °C. PP7CP-HF bound to RAT-tagged *SAMMSON* RNA-protein complexes was captured by the beads. After five washes with lysis buffer and once with lysis buffer without IGEPAL-CA630, RAT-tagged *SAMMSON* or its derivative bound with its associated proteins were eluted from the beads with 500 μg mL^{-1} FLAG peptide in the same buffer.

RT–qPCR

RNA was extracted with QIAzol lysis reagent (Qiagen) or with Nucleospin RNA/protein kit (Macherey-Nagel). RNA was reverse transcribed using the High-Capacity cDNA Reverse Transcription Kit (Thermo Fisher Scientific). *SAMMSON*, *TERRA*, *MALAT1*, *LINC00698*, *p32*, *COX1*, *ND1*, 18S, 16S and 12S expression was measured by qPCR on a LightCycler 480 (Roche) and normalized in qbase+ 3.0 (Biogazelle) using *HPRT1*, *TBP* and *UBC* as reference genes. Sequences of the primers are indicated in Supplementary Table 1.

Northern blotting

Nuclear pre-rRNA processing analysis was conducted as previously described 52. For northern blot analysis of mitochondrial pre-rRNAs, 4 μg of total RNA was subjected to 0.9 % agarose-formaldehyde gel electrophoresis in 3-(N-morpholino)propanesulfonic acid running buffer, and the separated RNAs were transferred to a Hybond-N+ membrane (GE Healthcare). The membrane was dried and subsequently cross-linked at 120 mJ cm^{-2}. After being stained with methylene blue, the membrane was hybridized to biotin-labeled DNA probe at 42 °C overnight in PerfectHyb Plus hybridization buffer (Sigma-Aldrich) according to the manufacturer's instructions. The hybridized membrane was washed sequentially with 2× SSC containing 0.1% SDS at 25 °C for 5 min, 0.5× SSC containing 0.1% SDS at 50 °C for 20 min, and 0.1× SSC containing 0.1% SDS at 25 °C for 20 min. The hybridized RNAs were detected using a Chemiluminescent Nucleic Acid Detection Module kit (Thermo Fisher Scientific) according to the manufacturer's instructions. RNA signals were detected using LAS4000 image analyzer and the signal intensities of RNA bands were quantified by Image J software.

Library preparation, small RNA-seq and data processing

Small RNA libraries were generated using the TruSeq small RNA library prep kit (Illumina) on 100 ng of input RNA according to the manufacturer's instructions. Size selection was performed using a pippin prep device (Sage Science). Libraries were quantified using a BioAnalyser (Agilent) and sequenced on a NextSeq500 (Illumina).

Small RNAs were quantified using Biogazelle's dedicated small RNA-seq pipeline (part of Cobra). Adaptors were trimmed using Cutadapt, discarding reads shorter than 15 nt and reads without adaptors.

Read quality was evaluated using the FASTX-Toolkit, applying a minimum quality score of 20 in at least 80% of bases. Reads were mapped using Bowtie without allowing mismatches. Mapped reads were subsequently annotated by matching genomic coordinates of each read with genomic locations of miRNAs (obtained from miRBase, v2053) and other small RNAs (obtained from UCSC and Ensembl54,55).

SUNsET

SUNsET was performed as described35. Briefly, ≈80% confluent cells were washed twice in 1× PBS and subsequently pulsed with puromycin-containing media (InvivoGen, 10 μg mL $^{-1}$) for 10 min. Due to the fact that puromycin is a structural analogue of aminoacyl tRNAs, it gets incorporated into the nascent polypeptide chain and prevents elongation. Thus, when used for reduced amounts of time, puromycin incorporation in neosynthesized proteins directly reflects the rate of mRNA translation in vitro. Puromycin incorporation was measured by western blotting using an antibody that recognises puromycin.

Click-iT® Metabolic Labeling for Protein

Click-iT protein labelling (Invitrogen) was performed according to the manufacturer's instruction. Cells were incubated for 1 h in methionine-free medium. Afterwards, 50 μM AHA were added to the media for 3 h. The signal was detected using an HRP-conjugated streptavidin antibody (ab7403, Abcam, 1:20,000).

Cellular fractionation and mitoplast isolation

Briefly, mitochondria were purified from 4-6 × 10^7 cells using mitochondria isolation kit for cultured cells (Thermo Fisher Scientific) according to manufacturer instructions, all buffers were supplemented with 60 U mL^{-1} Superase-In (Ambion) and 1× Halt Protease and Phosphatase Inhibitor Single-Use Cocktail (Life Technologies)). Mitoplasts were obtained by incubating purified mitochondria in RNase A-containing hypotonic buffer (HEPES pH 7.2 supplemented with 1× Halt Protease and Phosphatase Inhibitor Single-Use Cocktail (Life Technologies) and 10 μg mL^{-1} RNase A (Roche)) for 20 min on ice and subsequently incubated for 10 additional min at room temperature in order to remove all possible RNA contaminants. The purified mitoplasts were then washed thrice with Mitoplast Isolation Buffer (MIB: 250 nM Mannitol, 5 mM HEPES pH 7.2, 0.5 mM EGTA, 1 mg mL^{-1} BSA supplemented with 60 U mL^{-1} Superase-In (Ambion) and 1× Halt Protease and Phosphatase Inhibitor Single-Use Cocktail (Life Technologies)). For proteinase K experiments, purified mitochondria were resuspended in 1× sucrose buffer (SB: HEPES 10 mM, sucrose 280 mM, EGTA 1 mM pH 7,4) supplemented with 100 μg mL^{-1} proteinase K (Sigma-Aldrich) and with 60 U mL^{-1} Superase-In (Ambion) for 30 min at 4 °C rotating. Mitochondria were then pelleted at 9,000 *x*g for 10 min. Afterwards, mitochondria were resuspended in 1× SB supplemented with 20 nM PMSF (Sigma-Aldrich) and with 60 U mL^{-1} Superase-In (Ambion) and pelleted at 9,000 *x*g for 10 min. An additional washing step was performed with 1× SB supplemented with 20 nM PMSF (Sigma-Aldrich) and 1× Halt Protease and Phosphatase Inhibitor Single-Use Cocktail (Life Technologies) and with 60 U mL^{-1} Superase-In (Ambion). RNA and protein were then extracted with Nucleospin RNA/protein kit (Macherey-Nagel). Mitochondria and mitoplast enrichment was validated by RT-qPCR for the 16S mt-rRNA and by western blot using antibodies directed against multiple

mitochondrial proteins and calreticulin or calnexin (in order to exclude the possibility of ER contaminants). The same amount of proteins was loaded on the gel for each fraction to compare the enrichment of the different fractions.

Antibodies

Western blotting experiments were performed using the following primary antibodies: vinculin (V9131, clone hVIN-1 Sigma-Aldrich, 1:10,000), GAPDH (ab9485, Abcam, 1:1,000 or AM4300, clone 6C5, Ambion, 1:20,000), β-actin (sc-69879, clone AC-15, Santa Cruz Biotechnology, 1:2,000), p32 (A302-863A, Bethyl Laboratories, 1:5,000 or sc-10258, clone D-19, Santa Cruz Biotechnology, 1:1,000), XRN2 (A301-103A, Bethyl Laboratories, 1:2,000), CARF (A303-861A, Bethyl Laboratories, 1:2,000), NDUFS3 (Abcam 14711, 1:1,000), VDAC1 (ab3434-100, Abcam, 1:2,000), Hsp60 (BD611562, BD Biosciences, 1:5,000), Tom20 (FL-145, sc-11415, Santa Cruz Biotechnology, 1:1,000), calreticulin (C4606, Sigma-Aldrich, 1:10,000), calnexin (ab22595, Abcam, 1:5,000), SRSF1 (32-4600, Thermo Fisher Scientific, 1:250), puromycin (MABE343, clone 12D10, Merck-Millipore, 1:25,000), HA-tag (3724, clone C29F4, Cell Signaling Technologies, 1:1,000). The following HRP-linked secondary antibodies were used: anti-goat IgG (A5420, Sigma-Aldrich, 1:10,000), anti-mouse IgG (7076S, Cell Signaling Technologies, 1:5,000), anti-rabbit IgG (NA934-1ML, Sigma-Aldrich, 1:10,000).

FISH

For detection of *NEAT1* and the 12S at a single-cell level, pools of FISH probes were designed using the Stellaris probe designer software (Biosearch Technologies). Cells were grown on 8-well slides and fixed in 3.7% formahldeyde and permeabilised in 70% EtOH for >15 min at 4 °C. Hybridisation was carried out overnight at 37 °C in 2× SSC, 10% formamide and 10% dextran. Cells were counterstained with DAPI and visualized using an Olimpus Fluoview FV1200 using a LD635 laser for Cy5, LD559 HeNe for Cy3.5 and LD405 for DAPI.

Immunofluorescence

For immunofluorescence, cells were grown on 8-well slides and permeabilised in 1% BSA (Sigma-Aldrich) and 0.2% Triton X-100 (Sigma-Aldrich)-containing buffer for 10 min on ice. Blocking was performed in 1% BSA and 10% goat serum (DAKO) for 30 min at room temperature. Primary antibody incubation was performed at room temperature for 1 h. To detect p32, a rabbit antibody (A302-863A) from Bethyl Laboratories was used at a concentration of 1:1,000. To detect XRN2, a rabbit antibody (A301-103A) from Bethyl Laboratories was used at a concentration of 1:250. To detect CARF, a mouse antibody (H00055602-B01P) from Abnova was used at a concentration of 1:200. To detect puromycin, a mouse antibody (MABE343, clone 12D10) from Merck-Millipore was used at a concentration of 1:10,000. To detect fibrillarin, a mouse antibody (ABIN361375, clone 38F3) from Anticorps was used at a concentration of 1:500. Secondary antibody incubation was performed for 45 min at room temperature in the dark. As secondary antibodies, anti-rabbit or anti-mouse AlexaFluor-488 and AlexaFluor-647 (Life Technologies, 1:1,000) were used. MitoTracker™ Red CMXRos (Thermo Fisher Scientific) was added to the cells at a final concentration of 300 nM 30 min prior to fixation. Slides were then mounted with

Europe PMC Funders Author Manuscripts

ProLong Gold Antifade Mountant with DAPI (Thermo Fisher Scientific). Images where analysed on an Olympus Fluoview FW1200 using a LD635 laser for Cy5, LD559 HeNe for Cy3.5 and LD405 for DAPI.

Proximity Ligation Assay (PLA)

PLA Duolink® FarRed (Sigma-Aldrich) was performed following the manufacturer's instructions. To detect p32, a rabbit antibody (A302-863A) from Bethyl Laboratories was used at a concentration of 1:1,000. To detect CARF, a mouse antibody (H00055602-B01P) from Abnova was used at a concentration of 1:200. PLA® Probe Anti-Rabbit PLUS and PLA® Probe Anti-Mouse MINUS were used.

Xenografts

Animals were housed under pathogen-free conditions. All procedures involving animals (NMRI nude, female, 4 weeks old) were performed in accordance with the guidelines of the Catholic University of Leuven (KU Leuven) Animal Care and Use Ethical Committee (P147/2012). At the age of 4 weeks, mice were injected subcutaneously in either one or both flanks with 5×10^6 Mel-ST cells in 100 μL serum-free medium. Tumour volumes were calculated with the formula L × W × H × 0.42, where L is length, W is width and H is height.

Immunohistochemistry

Tumour samples were fixed in 3.7% PFA for 24 h at 4 °C, dehydrated with 70% EtOH for 24 h at 4 °C and subsequently rehydrated with demineralized water. The samples were then cut in sections of about 4 μm. Specimens were stained with haematoxylin and eosin and immunohistochemistry was performed using microwave pre-treatment of slides for antigen retrieval. Antibodies against Ki-67 (SP6, Thermo Fisher Scientific #RM-9106-S, clone SP6, 1:200) and puromycin (Merck Millipore, clone 12D10, 1:15,000) were applied, in conjunction with goat anti-rabbit horseradish peroxidase (HRP)-conjugated antibodies (DAKO) and visualized by DAB reaction. To evaluate the stainings, positive cells were counted using ImageJ.

Protein-RNA interactions (*cat*RAPID)

Interactions of *SAMMSON* to XRN2, CARF and p32 were predicted using catRAPID47,48, an algorithm that computes RNA-protein interactions by combining secondary structure, hydrogen bonding and van der Waals contributions. Background correction was obtained by subtracting the profile of AQP1, a *Bona fide* negative control, not retrieved in the mass spectrometry data from *SAMMSON* Pulldown).

Statistical analysis

The significance between means was determined by two-tailed paired Student's t test, with the exception of Figure 6b where two-way analysis of variation (ANOVA) was used and of Supplementary Figure 8c where two-tailed unpaired Student's t test was used. *P* values are represented as $P > 0.05$, not significant (*NS*); $P < 0.05$, *; $P < 0.01$, **; $P < 0.001$, ***; $P <$

0.0001, ****. All statistical analyses were performed with GraphPad Prism v7.0a (April 2, 2016) for Mac OS X.

Supplementary Material

Refer to Web version on PubMed Central for supplementary material.

Acknowledgments

GapmeRs were designed by J. Lai (Exiqon, Copenhagen Denmark). We would like to thank Marie Leucci for reading and editing the manuscript. This study was supported by the Fund Emile Carpentier – Fund André Vander Stricht – Fund Van Damme 2017-J1810830-207301. The authors wish to thank H. Brems for providing NHEM cultures, A. Sablina (VIB-KULeuven) for providing the SV40 LTA plasmid, M. Spinazzi (VIB-KULeuven) for the technical assistance and for sharing some antibodies, G. Ghanem (Jules Bordet Institute) for the patient derived melanoma cell line and somersault18:24 (http://www.somersault1824.com/) for providing some graphical illustrations. RV is recipient of FWO PhD fellowship 1S08316N. DL is supported by Fonds National de la Recherche (FRS/FNRS). GGT research is supported by European Research Council (RIBOMYLOME_309545), Spanish Ministry of Economy and Competitiveness (BFU2014-55054-P and BFU2017-86970-P).

References

1. Vander Heiden MG, Cantley LC, Thompson CB. Understanding the Warburg Effect: The Metabolic Requirements of Cell Proliferation. Science (80-). 2009; 324:1029–1033.
2. Wang M, Pestov DG. 5'-end surveillance by Xrn2 acts as a shared mechanism for mammalian pre-rRNA maturation and decay. Nucleic Acids Res. 2011; 39:1811–22. [PubMed: 21036871]
3. Teng T, Thomas G, Mercer CA. Growth control and ribosomopathies. Current Opinion in Genetics and Development. 2013; 23:63–71. [PubMed: 23490481]
4. Wu H, Sun H, Liang X, Lima WF, Crooke ST. Human RNase H1 is associated with protein P32 and is involved in mitochondrial pre-rRNA processing. PLoS One. 2013; 8:e71006. [PubMed: 23990920]
5. Ruggero D, Pandolfi PP. Does the ribosome translate cancer? Nat Rev Cancer. 2003; 3:179–192. [PubMed: 12612653]
6. Mayer C, Grummt I. Ribosome biogenesis and cell growth: mTOR coordinates transcription by all three classes of nuclear RNA polymerases. Oncogene. 2006; 25:6384–6391. [PubMed: 17041624]
7. Yang L, et al. Regulation of SirT1-nucleomethylin binding by rRNA coordinates ribosome biogenesis with nutrient availability. Mol Cell Biol. 2013; 33:3835–3848. [PubMed: 23897426]
8. Nishimura K, et al. Perturbation of Ribosome Biogenesis Drives Cells into Senescence through 5S RNP-Mediated p53 Activation. Cell Rep. 2015; 10:1310–1323. [PubMed: 25732822]
9. Schmidt O, Pfanner N, Meisinger C. Mitochondrial protein import: from proteomics to functional mechanisms. Nat Rev Mol Cell Biol. 2010; 11:655–67. [PubMed: 20729931]
10. Fogal V, et al. Mitochondrial p32 protein is a critical regulator of tumor metabolism via maintenance of oxidative phosphorylation. Mol Cell Biol. 2010; 30:1303–18. [PubMed: 20100866]
11. Skrtić M, et al. Inhibition of mitochondrial translation as a therapeutic strategy for human acute myeloid leukemia. Cancer Cell. 2011; 20:674–88. [PubMed: 22094260]
12. D'Andrea A, et al. The mitochondrial translation machinery as a therapeutic target in Myc-driven lymphomas. Oncotarget. 2016; 7:72415–72430. [PubMed: 27635472]
13. Battersby BJ, Richter U. Why translation counts for mitochondria - retrograde signalling links mitochondrial protein synthesis to mitochondrial biogenesis and cell proliferation. J Cell Sci. 2013; 126:4331–4338. [PubMed: 24013545]
14. Wang X, Chen XJ. A cytosolic network suppressing mitochondria-mediated proteostatic stress and cell death. Nature. 2015; 524:481–4. [PubMed: 26192197]
15. Wrobel L, et al. Mistargeted mitochondrial proteins activate a proteostatic response in the cytosol. Nature. 2015; 524:485–488. [PubMed: 26245374]

16. Rosenwald IB. The role of translation in neoplastic transformation from a pathologist's point of view. Oncogene. 2004; 23:3230–3247. [PubMed: 15094773]
17. Ruggero D. The role of Myc-induced protein synthesis in cancer. Cancer Research. 2009; 69:8839–8843. [PubMed: 19934336]
18. Fogal V, et al. Mitochondrial p32 is upregulated in Myc expressing brain cancers and mediates glutamine addiction. Oncotarget. 2015; 6:1157–70. [PubMed: 25528767]
19. Leucci E, et al. Melanoma addiction to the long non-coding RNA SAMMSON. Nature. 2016; 531:518–522. [PubMed: 27008969]
20. Tollervey D. Termination by torpedo. Nature. 2004; 432:456–457. [PubMed: 15565140]
21. Watanabe K, et al. Degradation of initiator tRNAMet by Xrn1/2 via its accumulation in the nucleus of heat-treated HeLa cells. Nucleic Acids Res. 2013; 41:4671–4685. [PubMed: 23471000]
22. Watanabe K, Ijiri K, Ohtsuki T. MTOR regulates the nucleoplasmic diffusion of Xrn2 under conditions of heat stress. FEBS Lett. 2014; 588:3454–3460. [PubMed: 25128458]
23. Petfalski E, Dandekar T, Henry Y, Tollervey D. Processing of the precursors to small nucleolar RNAs and rRNAs requires common components. Mol Cell Biol. 1998; 18:1181–9. [PubMed: 9488433]
24. Henras AK, Plisson-Chastang C, O'Donohue MF, Chakraborty A, Gleizes PE. An overview of pre-ribosomal RNA processing in eukaryotes. Wiley Interdisciplinary Reviews: RNA. 2015; 6:225–242. [PubMed: 25346433]
25. Preti M, et al. Gradual processing of the ITS1 from the nucleolus to the cytoplasm during synthesis of the human 18S rRNA. Nucleic Acids Res. 2013; 41:4709–4723. [PubMed: 23482395]
26. Sato S, et al. Collaborator of alternative reading frame protein (CARF) regulates early processing of pre-ribosomal RNA by retaining XRN2 (5′-3′ exoribonuclease) in the nucleoplasm. Nucleic Acids Res. 2015; 43:10397–10410. [PubMed: 26531822]
27. Gupta PB, et al. The melanocyte differentiation program predisposes to metastasis after neoplastic transformation. Nat Genet. 2005; 37:1047–1054. [PubMed: 16142232]
28. Boshuizen J, et al. Cooperative targeting of melanoma heterogeneity with an AXL antibody-drug conjugate and BRAF/MEK inhibitors. Nat Med. 2018; 24:203–212. [PubMed: 29334371]
29. Tripathi V, et al. The nuclear-retained noncoding RNA MALAT1 regulates alternative splicing by modulating SR splicing factor phosphorylation. Mol Cell. 2010; 39:925–938. [PubMed: 20797886]
30. Novo C, et al. The heterochromatic chromosome caps in great apes impact telomere metabolism. Nucleic Acids Res. 2013; 41:4792–4801. [PubMed: 23519615]
31. Livi CM, Klus P, Delli Ponti R, Tartaglia GG. CatRAPID signature: Identification of ribonucleoproteins and RNA-binding regions. Bioinformatics. 2015; 32:773–775. [PubMed: 26520853]
32. Richter U, et al. A mitochondrial ribosomal and RNA decay pathway blocks cell proliferation. Curr Biol. 2013; 23:535–41. [PubMed: 23453957]
33. West JA, et al. The Long Noncoding RNAs NEAT1 and MALAT1 Bind Active Chromatin Sites. Mol Cell. 2014; 55:791–802. [PubMed: 25155612]
34. Adriaens C, et al. P53 induces formation of NEAT1 lncRNA-containing paraspeckles that modulate replication stress response and chemosensitivity. Nat Med. 2016; 22:861–868. [PubMed: 27376578]
35. Schillewaert S, Wacheul L, Lhomme F, Lafontaine DLJ. The evolutionarily conserved protein Las1 is required for pre-rRNA processing at both ends of ITS2. Mol Cell Biol. 2012; 32:430–444. [PubMed: 22083961]
36. Tollervey D, Kiss T. Function and synthesis of small nucleolar RNAs. Current Opinion in Cell Biology. 1997; 9:337–342. [PubMed: 9159079]
37. Weinstein LB, Steitz JA. Guided tours: From precursor snoRNA to functional snoRNP. Current Opinion in Cell Biology. 1999; 11:378–384. [PubMed: 10395551]
38. Schmidt EK, Clavarino G, Ceppi M, Pierre P. SUnSET, a nonradioactive method to monitor protein synthesis. Nat Methods. 2009; 6:275–277. [PubMed: 19305406]

39. Pianese G, Teuscher R, Ziegler E. Beitrag zur Histologie und Aetiologie des Carcinoms: Histologische und experimentelle Untersuchungen. G. Fischer; 1896.
40. Bywater MJ, et al. Inhibition of RNA Polymerase I as a Therapeutic Strategy to Promote Cancer-Specific Activation of p53. Cancer Cell. 2012; 22:51–65. [PubMed: 22789538]
41. Quin JE, et al. Targeting the nucleolus for cancer intervention. Biochimica et Biophysica Acta - Molecular Basis of Disease. 2014; 1842:802–816.
42. Silvera D, Formenti SC, Schneider RJ. Translational control in cancer. Nat Rev Cancer. 2010; 10:254–266. [PubMed: 20332778]
43. Richter-Dennerlein R, Dennerlein S, Rehling P. Integrating mitochondrial translation into the cellular context. Nat Rev Mol Cell Biol. 2015; 16:586–592. [PubMed: 26535422]
44. Richter-Dennerlein R, et al. Mitochondrial Protein Synthesis Adapts to Influx of Nuclear-Encoded Protein. Cell. 2016; 167:471–483.e10. [PubMed: 27693358]
45. Richter U, Lahtinen T, Marttinen P, Suomi F, Battersby BJ. Quality control of mitochondrial protein synthesis is required for membrane integrity and cell fitness. J Cell Biol. 2015; 211:373–89. [PubMed: 26504172]
46. Delloye-Bourgeois C, et al. Nucleolar Localization of a Netrin-1 Isoform Enhances Tumor Cell Proliferation. Sci Signal. 2012; 5:ra57–ra57. [PubMed: 22871610]
47. Bellucci M, Agostini F, Masin M, Tartaglia GG. Predicting protein associations with long noncoding RNAs. Nature Methods. 2011; 8:444–445. [PubMed: 21623348]
48. Cirillo D, et al. Quantitative predictions of protein interactions with long noncoding RNAs: To the Editor. Nature Methods. 2016; 14:5–6. [PubMed: 28032625]
49. Ishikawa H, et al. Identification of truncated forms of U1 snRNA reveals a novel RNA degradation pathway during snRNP biogenesis. Nucleic Acids Res. 2014; 42:2708–2724. [PubMed: 24311566]
50. McHugh CA, et al. The Xist lncRNA interacts directly with SHARP to silence transcription through HDAC3. Nature. 2015; 521:232–236. [PubMed: 25915022]
51. Ishikawa H, et al. Truncated forms of U2 snRNA (U2-tfs) are shunted toward a novel uridylylation pathway that differs from the degradation pathway for U1-tfs. RNA Biol. 2018; 15:261–268. [PubMed: 29168419]
52. Tafforeau L, et al. The complexity of human ribosome biogenesis revealed by systematic nucleolar screening of pre-rRNA processing factors. Mol Cell. 2013; 51:539–551. [PubMed: 23973377]
53. Kozomara A, Griffiths-Jones S. MiRBase: Annotating high confidence microRNAs using deep sequencing data. Nucleic Acids Res. 2014; 42:D68–D73. [PubMed: 24275495]
54. Speir ML, et al. The UCSC Genome Browser database: 2016 update. Nucleic Acids Res. 2016; 44:D717–D725. [PubMed: 26590259]
55. Yates A, et al. Ensembl 2016. Nucleic Acids Res. 2016; 44:D710–D716. [PubMed: 26687719]

Europe PMC Funders Author Manuscripts

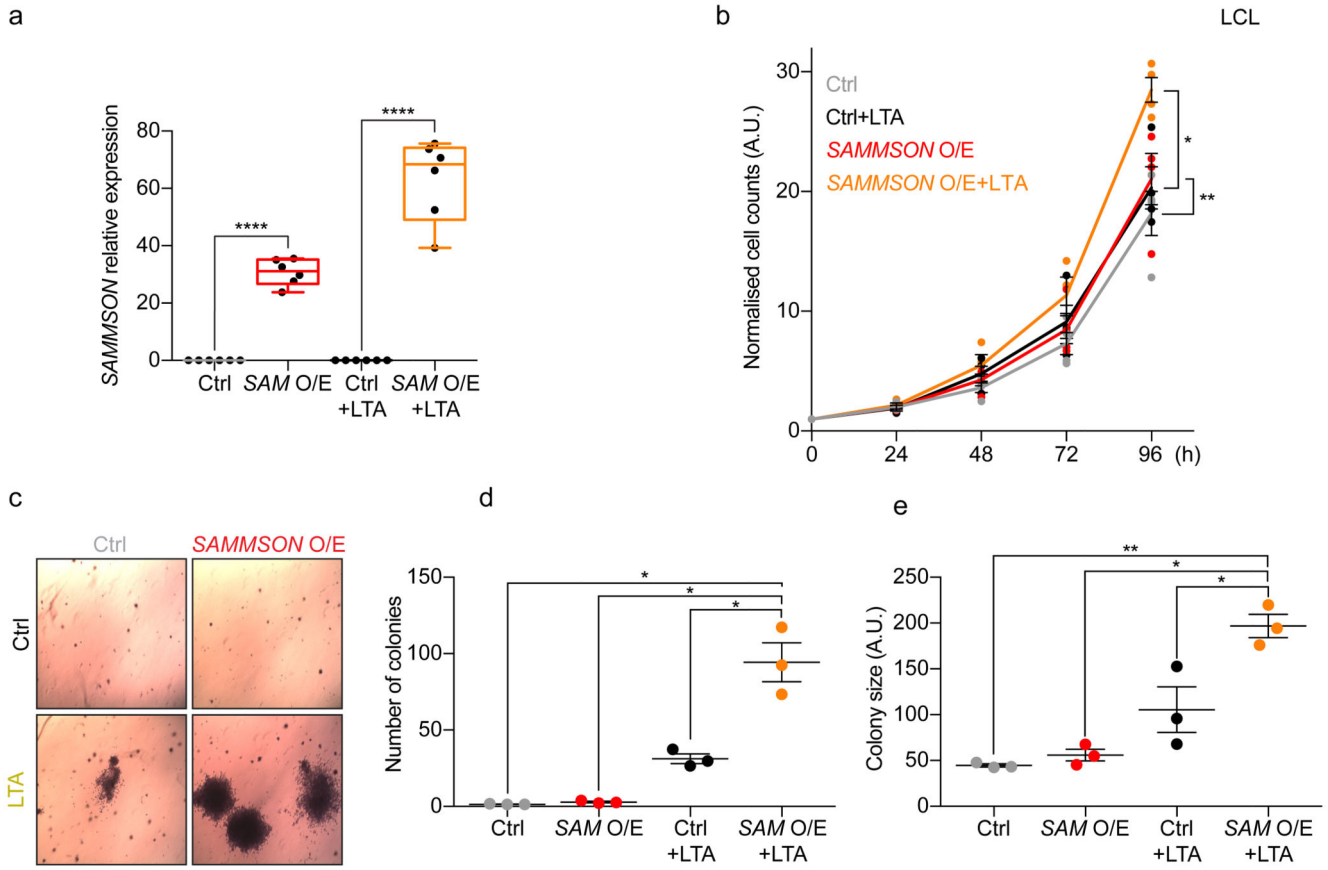

Figure 1. *SAMMSON* induces a malignant phenotype outside of the melanocytic lineage.

(**a**) *SAMMSON* relative expression measured by RT-qPCR in LCL cells infected with an empty (Ctrl) or a *SAMMSON*-encoding (*SAM* O/E) expression vector and/or with SV40 Large T Antigen (LTA); n=6. (**b**) Cell proliferation assays in LCL cells described in **a**. Error bars represent mean ± s.e.m.; n=4. (**c**) Soft agar assay in LCL cells described in **a**. Representative image of three independent experiments. (**d**) Quantification of number of colonies formed in soft agar as described in **c**. Error bars represent mean ± s.e.m.; n=3. (**e**) Quantification of colony size of soft agar colonies as described in **c**; Error bars represent mean ± s.e.m.; n=3. Box boundaries represent 25th and 75th percentiles; center line represents the median; whiskers, last data point within ±1.5 interquartile range. *P* values were calculated by paired two-tailed Student's t-test. * $P<0.05$; ** $P<0.01$; **** $P<0.0001$.

Europe PMC Funders Author Manuscripts

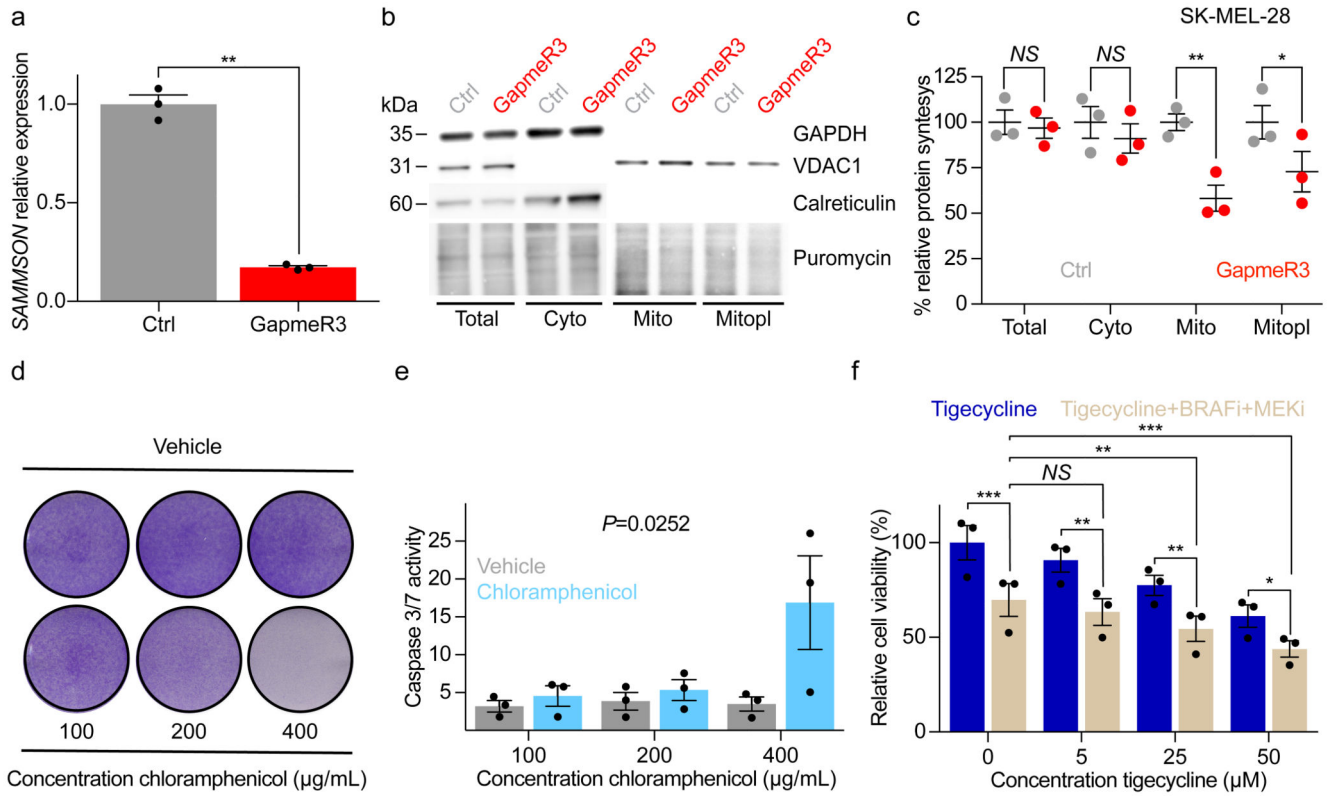

Figure 2. Desynchronization of cytosolic and mitochondrial translation machinery decreases melanoma cell fitness and can be therefore exploited therapeutically.

(**a**) *SAMMSON* relative expression measured by RT-qPCR in SK-MEL-28 cells transfected with a non-targeting GapmeR(Ctrl) or GapmeR3. Error bars represent mean ± s.e.m.; n=3. (**b**) Western blotting after a 10-minute pulse with puromycin and subsequent cytosol(Cyto)-mitochondria (Mito)-mitoplast(Mitopl) fractionation in SK-MEL-28 cells described in **a**. Representative images of three independent experiments. (**c**) Quantification of relative protein synthesis (%) in SK-MEL-28 cells as described in **a** and **b**. Error bars represent mean ± s.e.m.; n=3. (**d**) Colony formation assays 5 days after seeding $1'\ 10^3$ SK-MEL-28 cells and treating them with increasing amounts of chloramphenicol or vehicle (EtOH). The violet colour is given by crystal violet, a compound that binds intracellular DNA and protein thus highlighting the cells in the plate. Representative image of three independent experiments. (**e**) Caspase 3/7 activity 72 hours after treating SK-MEL-28 cells with increasing amounts of chloramphenicol or vehicle (EtOH). Error bars represent mean ± s.e.m.; n=3. *P* values was calculated with two-way ANOVA. (**f**) Relative cell viability of MM099 cells measured 48 hours after treatment with either Tigecycline or a combination of Tigecycline, BRAFi (Dabrafenib) and MEKi (Trametinib). Error bars represent mean ± s.e.m.; n=3. *P* values were calculated by paired two-tailed Student's t-test. * $P<0.05$; ** $P<0.01$; *** $P<0.001$; *NS*, not significant. Uncropped gel images are shown in Supplementary Data Set 1.

Europe PMC Funders Author Manuscripts

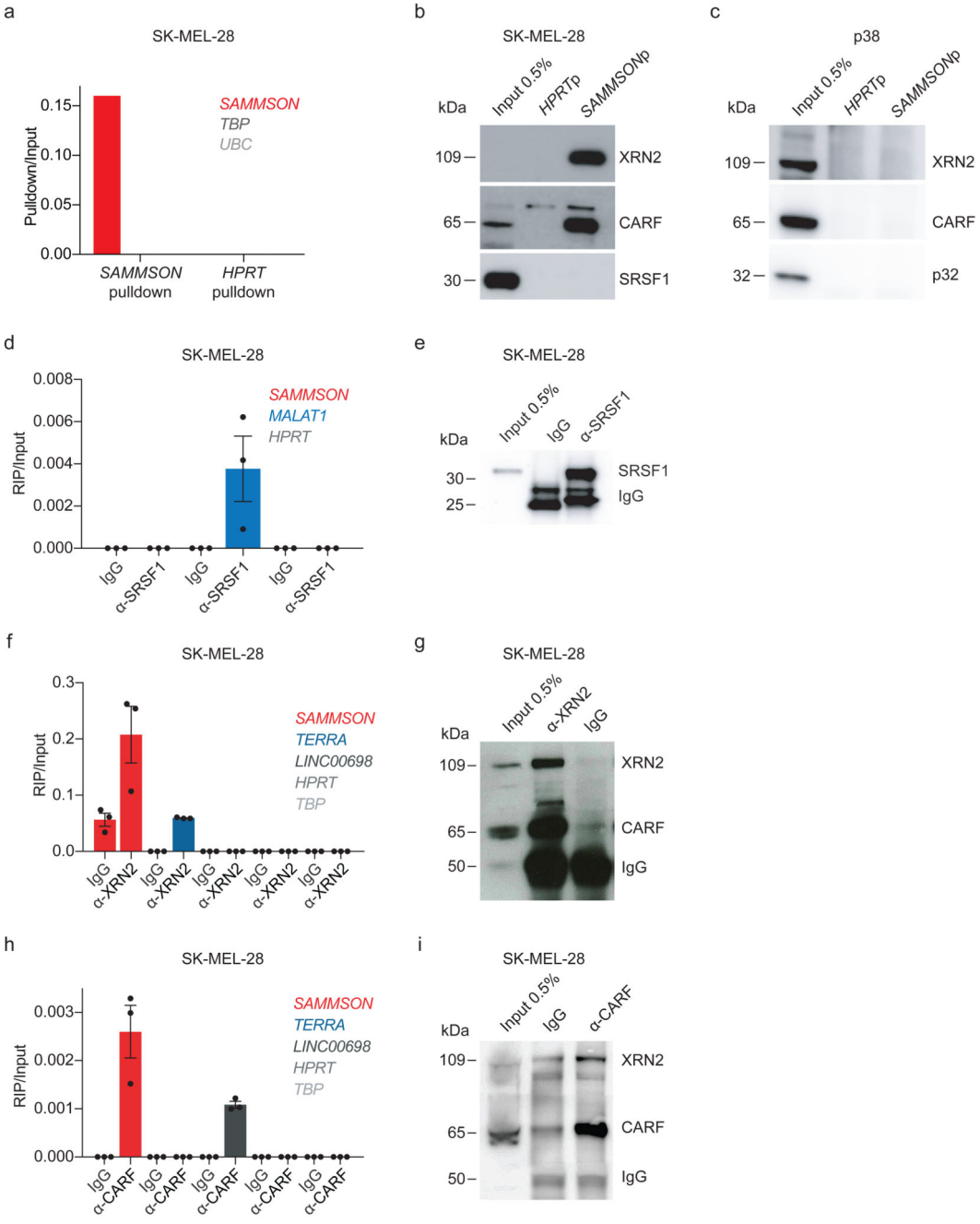

Figure 3. *SAMMSON* interacts with XRN2 and CARF.

(**a**) *SAMMSON* (but not *TBP* or *UBC*) is specifically recovered by RAP after UV crosslinking SK-MEL-28 cells. Representative image of three independent experiments. (**b**) *SAMMSON* and *HRPT* pulldown in native conditions (using two sets of 48 biotinylated probes recognizing mature transcripts, *p*) and western blotting in SK-MEL-28 cells. Representative image of three independent experiments. (**c**) *SAMMSON* and *HRPT* pulldown in native conditions (using biotinylated probes, *p*) and western blotting in mouse p38 cells. Representative image of three independent experiments. (**d**) *MALAT1* (but not

Europe PMC Funders Author Manuscripts

SAMMSON or *HPRT*) is recovered by RIP using an SRSF1- specific antibody as measured by RT-qPCR in SK-MEL-28 cells. Error bars represent mean ± s.e.m.; n=3. (**e**) Western blot confirming enrichment of SRSF1 following RIP with an anti- SRSF1 antibody in SK-MEL-28 cells. Representative image of three independent experiments. (**f**) *SAMMSON* and *TERRA* are recovered by RIP using an XRN2-specific antibody as measured by RT-qPCR in SK-MEL-28 cells. Error bars represent mean ± s.e.m.; n=3. (**g**) Western blot confirming enrichment of XRN2 (and CARF) following RIP with an anti-XRN2 antibody in SK-MEL-28 cells. Representative image of three independent experiments. (**h**) *SAMMSON* and *LINC00698* are recovered by RIP using a CARF-specific antibody as measured by RT-qPCR in SK-MEL-28 cells. Error bars represent mean ± s.e.m.; n=3. (**i**) Western blot confirming enrichment of CARF (and XRN2) following RIP with an anti-CARF antibody in SK-MEL-28 cells. Representative image of three independent experiments. Uncropped gel images are shown in Supplementary Data Set 1.

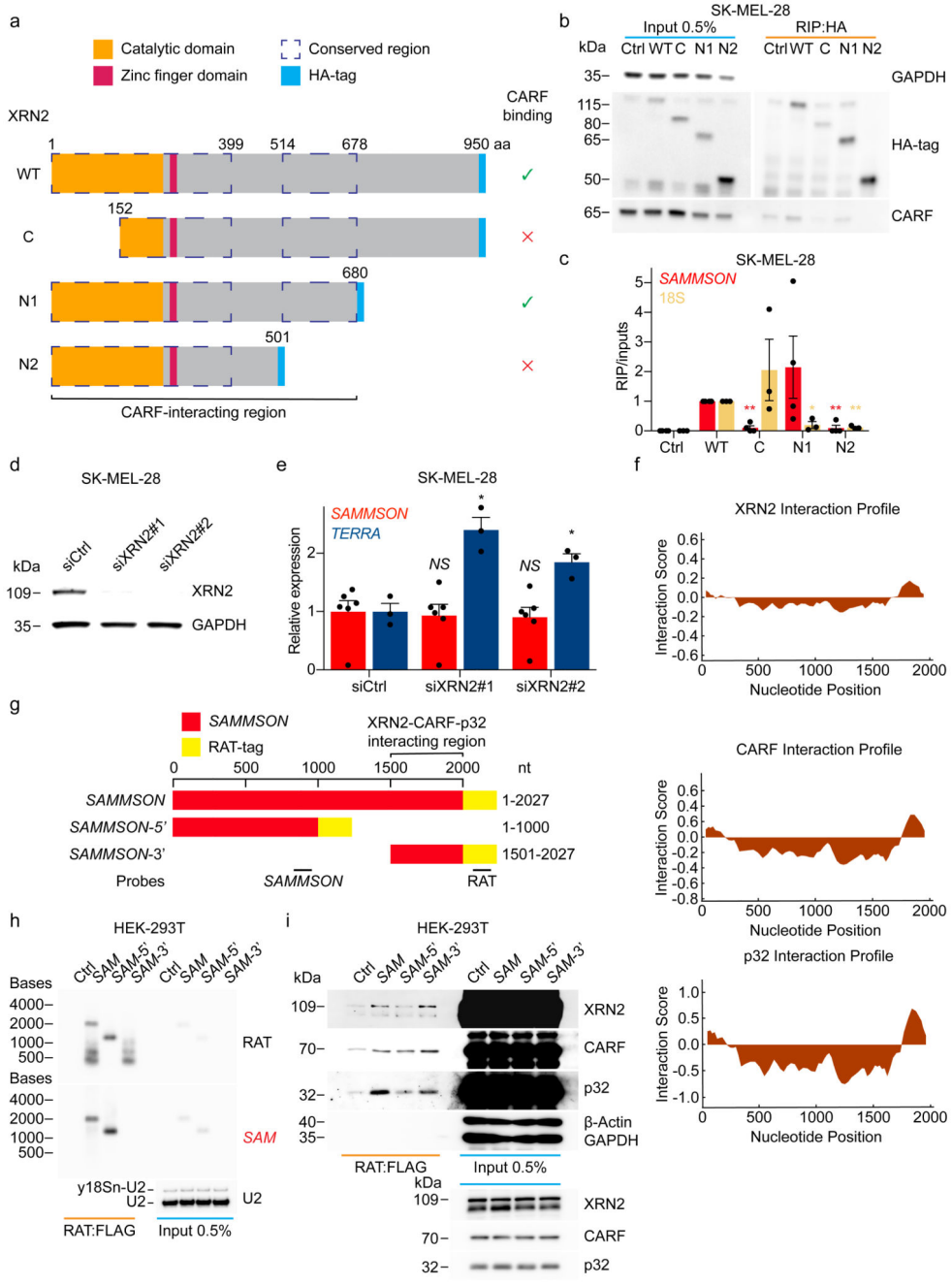

Figure 4. Identification of *SAMMSON*-binding region on XRN2 and of *SAMMSON* protein-binding domain.

(**a**) Schematic representation of the different HA-XRN2-constructs. (**b**) Western blot confirming enrichment of XRN2 (and CARF) in SK-MEL-28 cells transfected with different XRN2 constructs or an untransfected control (Ctrl) followed by RIP with an anti- HA-tag antibody. Representative images of four independent experiments. (**c**) *SAMMSON* and 18S are recovered by RIP using a HA-tag-specific antibody only in one out of the three XRN2 deletion constructs (N1 and C respectively) as measured by RT-qPCR in SK-MEL-28 cells.

Europe PMC Funders Author Manuscripts

All deletion mutants were normalised on the positive control (WT) sample. Red asterisks refer to *SAMMSON* significance (paired two-tailed Student's t-test WT vs the deletion mutants), yellow asterisks refer to 18S significance (paired two-tailed Student's t-test WT vs the deletion mutants). Error bars represent mean ± s.e.m.; *SAMMSON*, n=4; 18S, n=3. (**d**) Western blotting of SK-MEL-28 cells 72 hours after transfection with a control siRNA (siCtrl) or two different siRNAs targeting XRN2 (siXRN2#1 and siXRN2#2). Representative images of six independent experiments. (**e**) *SAMMSON* and *TERRA* relative expression as measured by RT- qPCR in SK-MEL-28 cells treated as described in **d**. Error bars represent mean ± s.e.m.; *SAMMSON*, n=6; *TERRA*, n=3. **(f)** Binding of *SAMMSON* to XRN2, CARF and p32 were predicted using the *cat*RAPID47,48. Background correction was obtained by subtracting the profile of a *bona fide* negative control. (**g**) Schematic representation of the different *SAMMSON*_RAT-tag constructs **(h)** FLAG-tag RIP in HEK-293T cells transfected either with the different *SAMMSON* constructs or control plasmid (Ctrl) followed by northern blot using the probes for the RAT-tag and *SAMMSON* indicated in **g**. Representative images of three independent experiments. **(i)** Western blot with the protein fraction recovered from the RIP described in **h**. Top panel long exposure, bottom panel short exposure (for 0.5% Input only). Representative images of three independent experiments. *P* values were calculated by paired two-tailed Student's t-test. * $P<0.05$; ** $P<0.01$; *NS*, not significant. Uncropped gel images are shown in Supplementary Data Set 1.

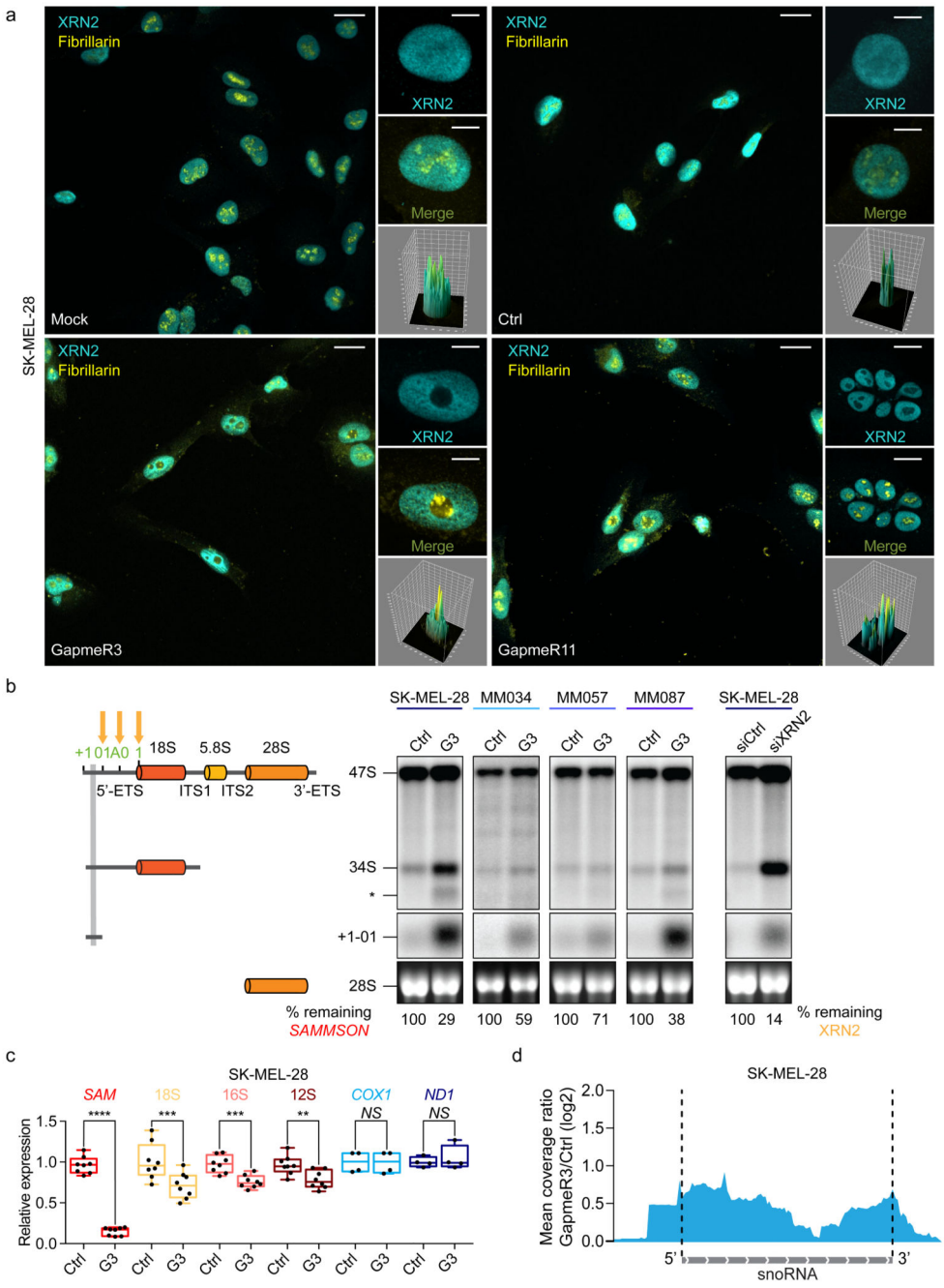

Figure 5. *SAMMSON* modulates XRN2 localization and function.

(**a**) Representative XRN2 (cyan) and fibrillarin (yellow) IF in SK-MEL-28 cells 30 hours after transfection with a non-targeting GapmeR(Ctrl), GapmeR3 or GapmeR11 or untransfected (Mock). Scale bar low magnification, 10 μm; high magnification, 2 μm. Representative images of three independent experiments. **(b)** Left, schematic representation of the pre-rRNAs and the mature rRNAs detected by northern blotting, the orange arrows indicate the sites of pre-rRNA processing inhibition in the 5'-ETS (01, A0, and 1). The probe used is highlighted in grey. ETS: external transcribed spacers; ITS: internal transcribed

spacers. The aberrant 34S RNA is produced when cleavage occurs in ITS1 prior to 5'-ETS. *, truncated form of the 34S RNA. Right, northern blot hybridization analysis of pre-rRNA isolated from four melanoma cell lines (with different mutational backgrounds and phenotype) transfected with a non- targeting GapmeR (Ctrl) or a GapmeR3 (G3) or of SK-MEL-28 transfected with a XRN2- targeting (siXRN2) or control (siCtrl) siRNA. KD efficiency is shown for both *SAMMSON* KD and XRN2 KD. Representative image of three independent experiments. (**c**) *SAMMSON* (*SAM*), 18S, 16S, 12S, Cyclooxygenase 1 (*COX1*) and NADH-ubiquinone oxidoreductase chain 1 (*ND1*) relative expression measured by RT-qPCR in SK- MEL-28 cells 30 hours after transfection with a non-targeting GapmeR (Ctrl) or with GapmeR3 (G3); n=8 for *SAMMSON*, 18S, 16S and 12S; n=4 for *COX1* and *ND1*. **(d)** Mean coverage ratio between *SAMMSON* KD and a non-targeting GapmeR across all expressed snoRNAs. Data are displayed for a snoRNA meta-gene, demonstrating increased coverage beyond the snoRNA boundaries. Box boundaries represent 25th and 75th percentiles; center line represents the median; whiskers, last data point within ±1.5 interquartile range. *P* values were calculated by paired two-tailed Student's t-test. ** $P<0.01$; *** $P<0.001$; **** $P<0.0001$; *NS*, not significant. Uncropped gel images are shown in Supplementary Data Set 1.

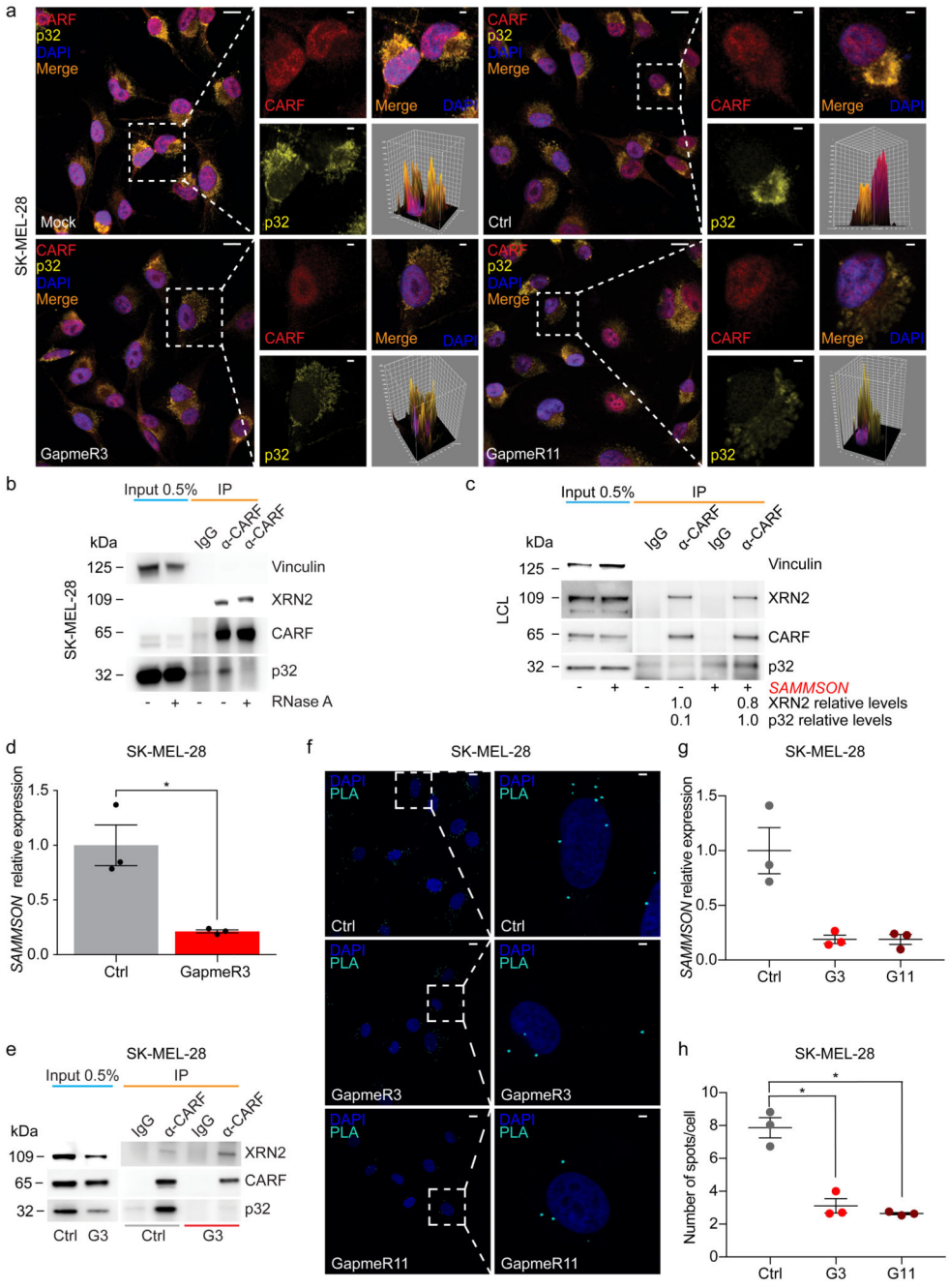

Figure 6. *SAMMSON* promotes CARF localization to the cytoplasm and its binding to p32.

(**a**) Representative CARF (red) and p32 (yellow) IF in SK-MEL-28 cells 30 hours after transfection with a non-targeting GapmeR(Ctrl), GapmeR3 or GapmeR11 or untransfected (Mock). Cell nuclei are stained with DAPI (blue). Scale bar low magnification, 10 μm; high magnification, 2 μm. Representative images of three independent experiments. (**b**) CARF IP in SK-MEL-28 cells in the presence (+) or absence (-) of RNase A and western blotting. Representative image of three independent experiments. (**c**) CARF IP in LCL cells described in Figure 1a and western blotting, where (-) represents cells infected with an empty control

plasmid and (+) the *SAMMSON*-expressing cells. Representative image of three independent experiments. (**d**) *SAMMSON* relative expression measured by RT-qPCR in SK-MEL-28 cells 30 hours after transfection with a non-targeting GapmeR (Ctrl) or GapmeR3 (G3). Error bars represent mean ± s.e.m.; n=3. (**e**) CARF IP in SK-MEL-28 cells treated as described in **d** and western blotting. Representative images of three independent experiments. **(f)** Representative Proximity Ligation Assay (PLA, cyan) assay using antibodies against CARF and p32 in SKMEL-28 cells 30 hours after transfection with a non-targeting (Ctrl), GapmeR3 or GapmeR11. Cell nuclei are stained with DAPI (blue). Scale bar low magnification, 10 μm; high magnification, 2 μm. Representative images of three independent experiments. (**g**) *SAMMSON* relative expression measured by RT-qPCR in SK-MEL-28 cells 30 hours after transfection with a non-targeting GapmeR(Ctrl), GapmeR3 (G3) or GapmeR11 (G11). Error bars represent mean ± s.e.m.; n=3. (**h**) Quantification of PLA assay described in **f** and **g**. Error bars represent mean ± s.e.m.; n=3. *P* values were calculated by paired two-tailed Student's t-test. * $P<0.05$. Uncropped gel images are shown in Supplementary Data Set 1.

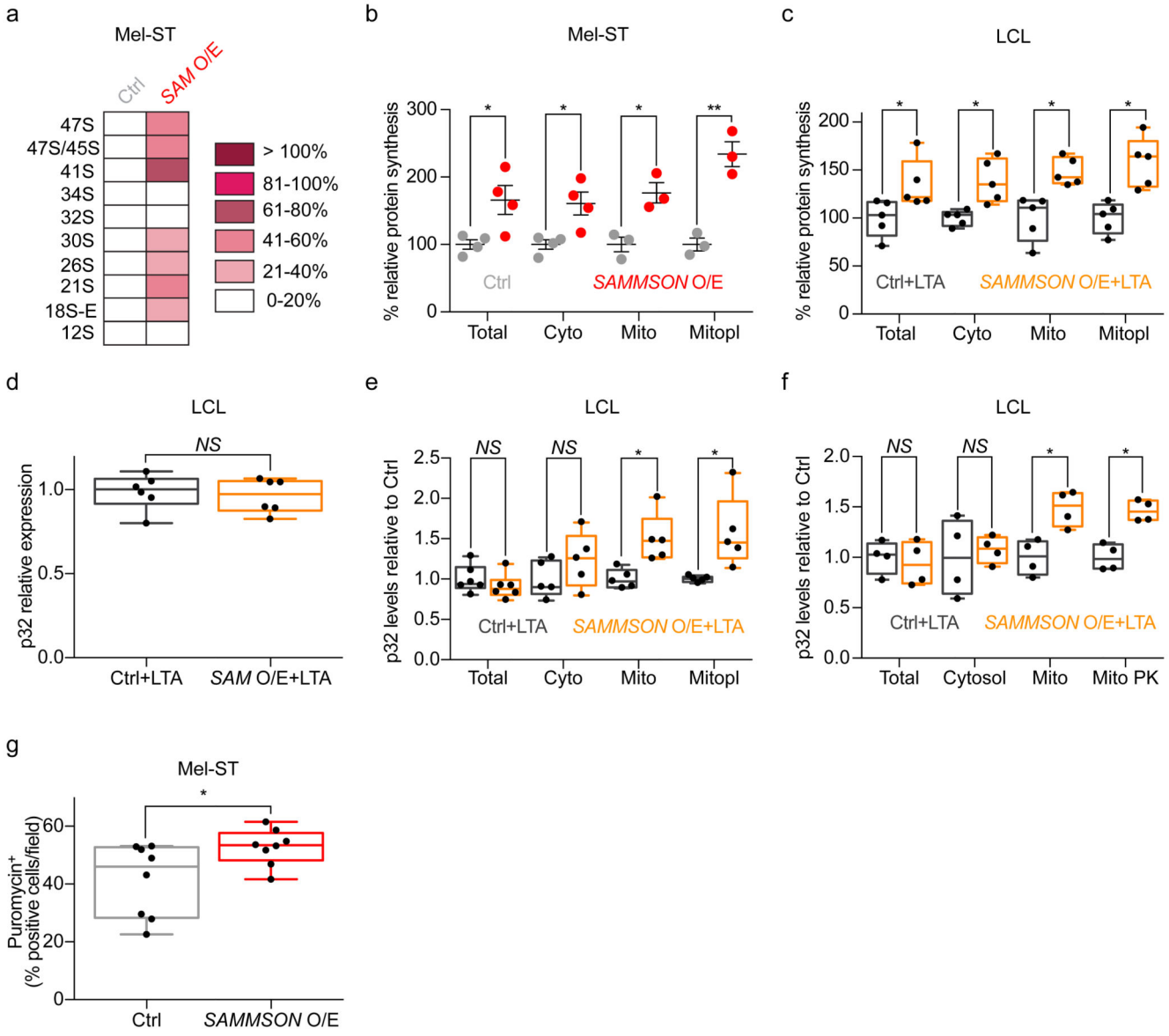

Figure 7. *SAMMSON* expression increases rRNA processing thus promoting protein synthesis.

(**a**) Heatmap representation of pre-rRNA analysis in Mel-ST cells overexpressing *SAMMSON* (*SAM* O/E) relative to cells transfected with an empty (Ctrl). Each pre-RNA intermediates detected was quantified with a PhosphorImager; n=3. (**b**) Quantification of relative protein synthesis (%) after a 10-minute pulse with puromycin and subsequent cytosol(Cyto)-mitochondria(Mito)-mitoplast(Mitopl) fractionation in Mel-ST cells described in **a**. Error bars represent mean ± s.e.m. Total and Cyto, n=4; Mito and Mitopl, n=3. (**c**) Quantification of relative protein synthesis (%) after a 10-minute pulse with puromycin and subsequent cytosol(Cyto)-mitochondria(Mito)-mitoplast(Mitopl) fractionation in LCL cells as described in Figure 1a; n=5. (**d**) *p32* relative expression measured by RT-qPCR in LCL cells as described in **c**; n=6. (**e**) Quantification of p32 protein levels relative to the control fraction in LCL cells described in **c** after cytosol(Cyto)-mitochondria(Mito)-

Europe PMC Funders Author Manuscripts

mitoplast(Mitopl) fractionation; n=6. (**f**) Quantification of p32 protein levels relative to the control fraction after cytosol(Cyto)-mitochondria(Mito)-proteinase K-treated mitochondria(Mito+PK) fractionation in LCL cells as described in Figure 1a; n=4. (**g**) Puromycin quantification (each point represents the average of the quantification of three different fields) of tumors as described in Figure 1e-g; n=8. Box boundaries represent 25th and 75th percentiles; center line represents the median; whiskers, last data point within ±1.5 interquartile range. *P* values were calculated by paired two-tailed Student's t-test. * $P<0.05$; ** $P<0.01$; *NS*, not significant.

Europe PMC Funders Author Manuscripts

Europe PMC Funders Author Manuscripts

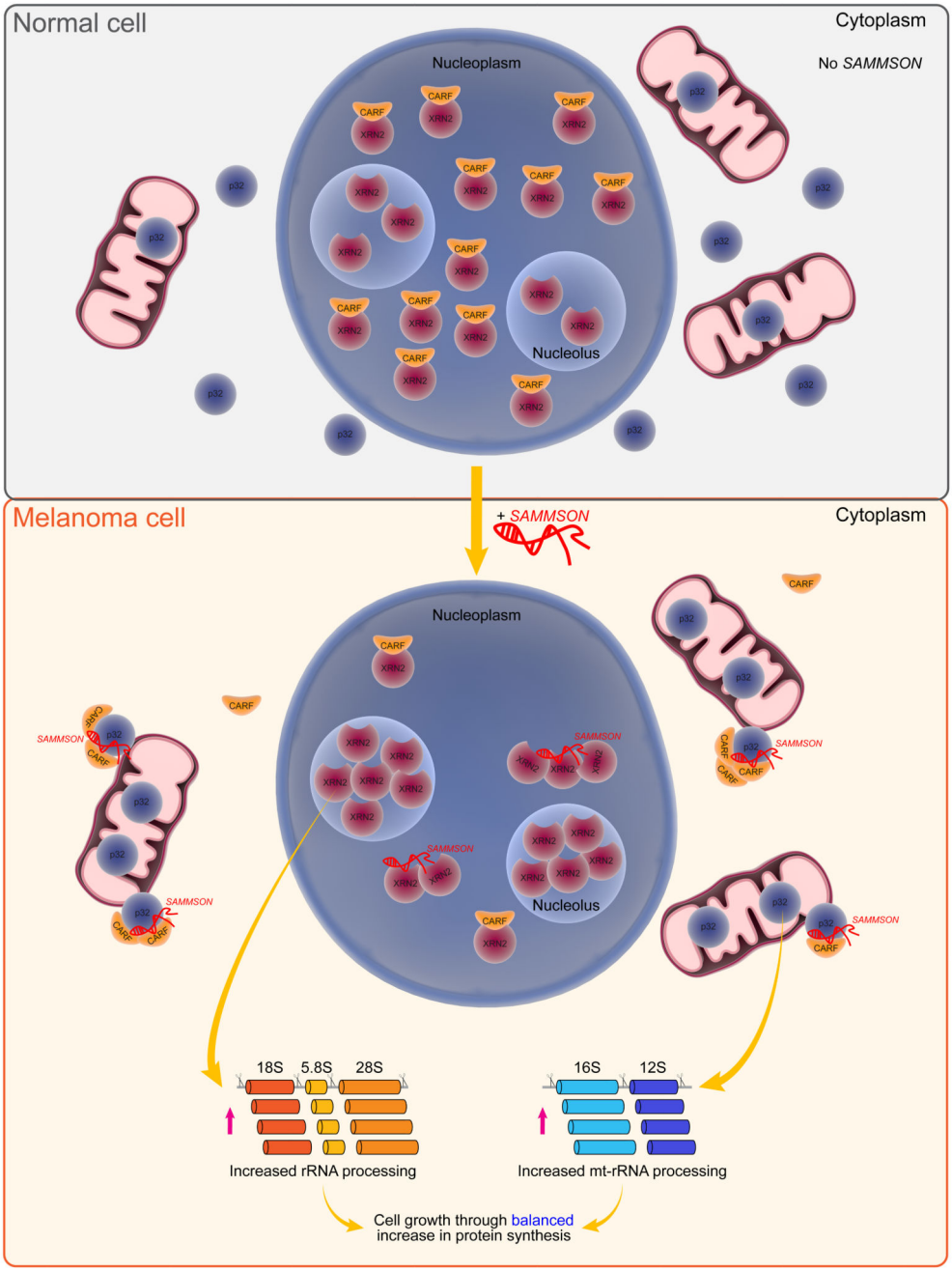

Figure 8. Schematic representation of *SAMMSON* mechanism of action.

In normal (*SAMMSON*-negative) cells, CARF controls the nuclear localization of XRN2 by sequestering a pool of it in the nucleoplasm. In the context of melanoma, *SAMMSON* expression promotes the interaction of CARF with p32 at the expense of the CARF-XRN2 interaction, thus favoring p32 mitochondrial localization and XRN2 nucleolar localization. By modulating these interactions *SAMMSON* determines a balanced increase in rRNA

maturation and protein synthesis in the cytosol and mitochondria. As a result, *SAMMSON* promotes an increase in cell growth.

Europe PMC Funders Author Manuscripts